



CaTiO₃-hydroxyapatite bioceramic composite: Synthesis of reactant powders from waste cockle shell, sintering, characterization and investigation of physical, mechanical and *in-vitro* biological properties

Siriwadee Sri-o-Sot¹ · Klatnatee Vepulanont² · Thanawat Pitakpornpreecha³ · Aratee Aroonkesorn³ · Adisri Charoenpanich⁴ · Thapanee Srichumpong⁵ · Tawat Chanadee¹

Received: 17 September 2023 / Revised: 15 November 2023 / Accepted: 12 December 2023 / Published online: 20 December 2023
© The Author(s) under exclusive licence to Australian Ceramic Society 2023

Abstract

Calcium titanate-hydroxyapatite composites (CT-HAp) were synthesized using a conventional sintering process. The calcium source was derived from cockle shell waste. The combustion synthesis of CT (CaTiO₃) produced fine, irregular, sub-micron size particles. The precipitation synthesis of HAp (Ca₅(PO₄)₃OH) produced rod-like nanoparticles. The obtained powders were used to fabricate CT-HAp bioceramic composites sintered at 1250 °C for 2 h. The phase formation, microstructure, and physical and mechanical properties of HAp and various CT-HAp composites were investigated. A CT-HAp composite with 8%wt of CT, having a density of 3.00 ± 0.01 g/cm³ and a grain size of 0.90 ± 0.06 μm, produced the highest values for flexural strength, Vickers hardness and fracture toughness: 56.67 ± 1.122 MPa, 6.03 ± 0.02 GPa, and 7.77 MPa.m^{1/2}, respectively. The chemical solubility of the CT-HAp composites was very low, showing an average weight loss of 0.24% in a simulated body fluid solution. The properties of the CT-HAp composites were controlled by CT content and porosity. *In-vitro* biological studies demonstrated the growth and proliferation of MC3T3-E1 osteoblast cells on all composites after three days of culture. The highest cell viability was exhibited on a CT-HAp composite with a CT content of 8%wt. The expression of alkaline phosphatase (ALP) activity on the composite surface promoted cellular osteoinduction, indicating the potential of the developed composite for bone formation and repair.

Keywords Calcium titanate · Hydroxyapatite · Cockle shell · Bioactive ceramic · Osteoblast

Introduction

Calcium phosphate-based materials, especially hydroxyapatite (HAp)-based composites, are used in orthopedics and dentistry to repair or replace human bone and teeth [1] but the applications of these biomaterials are limited by the brittle nature of HAp. This limitation can be mitigated by the use of reinforcing materials, which are commonly metal oxides such as zirconium oxide (ZrO₂), aluminium oxide (Al₂O₃) and titanium oxide (TiO₂) [2].

An alternative approach that incorporates calcium titanate (CT, CaTiO₃) particles with HAp (Ca₅(PO₄)₃OH) has produced positive results in different processing conditions that have improved other material properties such as density, modulus, strength, hardness and fracture toughness as well as brittleness [1, 3–13]. Furthermore, CT improves the biocompatibility of the composite, producing a positive surface

✉ Tawat Chanadee
tawat.ch@psu.ac.th

¹ Program in Materials Science, Division of Physical Science, Faculty of Science, Prince of Songkla University, Hat Yai, Songkhla 90110, Thailand

² Program in Chemistry, Division of Physical Science, Faculty of Science, Prince of Songkla University, Hat Yai, Songkhla 90110, Thailand

³ Program in Biochemistry, Division of Health and Applied Sciences, Faculty of Science, Prince of Songkla University, Hat Yai, Songkhla 90110, Thailand

⁴ Department of Biology, Faculty of Science, Silpakorn University, Mueang, Nakhon Pathom 73000, Thailand

⁵ National Metal and Materials Technology Center (MTEC), Khlong Luang, Pathum Thani 12120, Thailand

charge which resembles the surface electrical property of natural bone [14]. CT is a good substrate for apatite growth, and promotes the osseointegration that plays an important role in connecting the surfaces of the living bone and the implant. CT hydrolyzes in simulated body fluid (SBF), producing numerous Ti–OH groups. During the incubation process, contact between the implant surface and osteoblast cells is enhanced, and the exchange of Ca^{2+} and $(\text{PO}_4)^{3-}$ ions is activated. In addition, TiO_3^{2-} from CT attracts calcium and phosphorus ions from surrounding bone tissue and body fluids to promote nucleation. CT also enhances interfacial bonding within bio-ceramics. These physical and chemical changes have been shown to induce apatite formation, and enhance regeneration and integration during repairing bone defect rehabilitation [1, 3–13].

The cockle is an edible marine bivalve mollusk that it has an economic value as seafood and is widely consumed in Southeast Asia. In 2021, the Department of Fisheries, Ministry of Agriculture and Cooperatives reported that there were 1,637 cockle farms in Thailand that produced 33,526.27 tons of cockles. A large volume of waste cockle shells from processing is produced, causing an environmental problem. Recycling this waste could contribute to the more sustainable development of marine resources. Previous studies demonstrated that cockle shells contain calcium carbonate (CaCO_3) in the crystal form of aragonite, consisting of 97% calcium (Ca) [15–17]. The proportion of CaO in commercial calcium carbonate is 99.10%wt [18], and the yield of CaO powder obtained from cockle shell after calcination is higher than that yielded by mussel and oyster shells [19]. Furthermore, cockle shells are used as a raw material in the synthesis of HAp by various methods [20–28]. However, the only shell that has been used to produce CT is the scallop shell [29]. Therefore, cockle shell is a potentially attractive, untapped, calcium source for the preparation of CT as well as HAp.

The present work aims to fabricate CT-HAp composites and improve their properties for biomedical applications. CT was synthesized by an energy-saving combustion synthesis method and HAp was prepared by a precipitation process. Reactant powders for both components were produced from waste cockle shell. The phase formation and morphology of the reactant powders and the fabricated CT-HAp composites were investigated. The CT-HAp composites were characterized and discussed in terms of physical, mechanical and biological properties.

Experimental procedures

Preparation of powders as a calcium source

Raw cockle shell for the present work was supplied by a seafood farm in Samut Songkhram Province on the Gulf of Thailand. X-ray fluorescence (XRF) analysis of the chemical

Table 1 The chemical composition of raw waste cockle shell

Compound	Concentration (%wt)
Al_2O_3	0.059
CaO	98.280
Cl	0.041
Fe_2O_3	0.248
MgO	0.061
Na_2O	0.578
P_2O_5	0.041
SiO_2	0.295
SO_3	0.133
SrO	0.264

Note: The result was normalized to 100% (LOI-free)

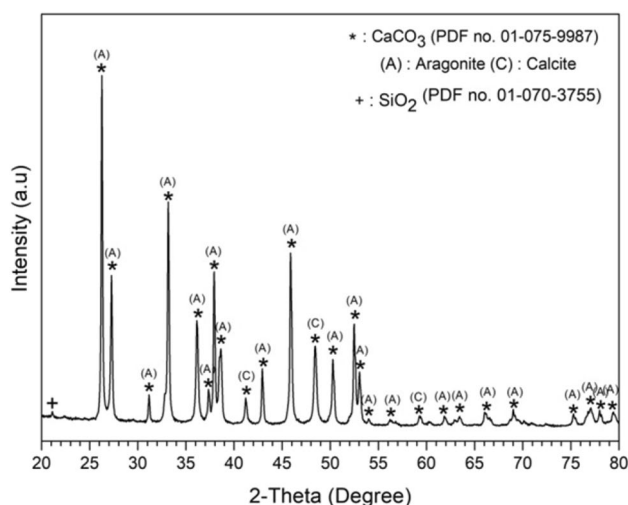


Fig. 1 XRD pattern of raw waste cockle shell used in this work

composition of the cockle shell (Table 1) showed that CaO was a major component in coexistence with other trace oxides.

The XRF analysis was confirmed by X-ray diffraction (XRD) analysis (Fig. 1), which indicated that the cockle shell was mainly composed of CaCO_3 and contained aragonite as a major crystalline form along with a minor phase of calcite. The XRD analysis detected SiO_2 , but not Na_2O , Fe_2O_3 and SrO that were detected by XRF analysis. Although Na_2O and SiO_2 were both detected in trace amounts, only the peak of SiO_2 was detected by XRD. Possibly the crystallinity of SiO_2 was more perfect than the crystallinity of Na_2O .

Since biomaterials are implanted in the living body, any toxic impurities must be identified. Therefore, arsenic (As), cadmium (Cd) and lead (Pb) contents were determined by inductively coupled mass spectrometry (ICP-MS), and mercury (Hg) content was determined by direct mercury analysis. No Hg and Cd were found, and although As

Table 2 The table compares the found contents of heavy metal elements in raw waste cockle shell with the relevant standards

Element	Concentration (ppm)		
	ASTM F1185-88	ISO 3779-1:2008	This work
As	3	<3	0.117 ± 0.012
Cd	5	<5	Undetected
Pb	30	<30	<0.100
Hg	5	<5	Undetected

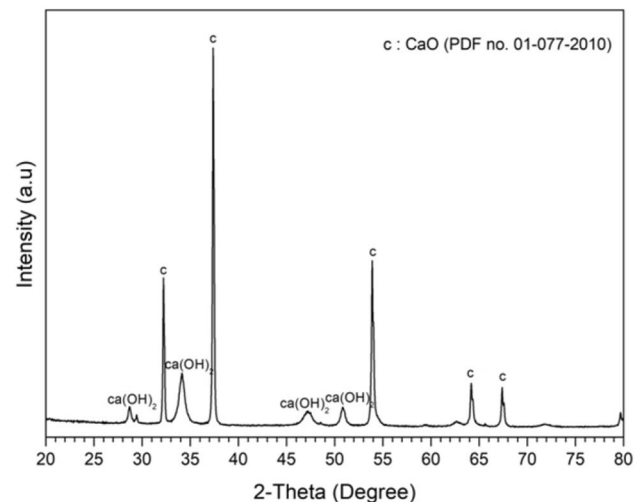
(0.117 ± 0.012 ppm) and Pb (<0.100 ppm) were detected, the detected levels were below the maximum limit permitted by the relevant standards (ASTM F1185-88 and ISO 3779-1:2008) (Table 2). Therefore, the raw cockle shell was considered suitable for use in biomedical applications.

Raw cockle shell was washed several times with distilled water and then immersed in hydrogen peroxide (H₂O₂, 30%, Chem-Supply) solution for 24 h to eliminate soluble inorganic contaminants. The cleaned cockle shell was dried in an oven at 110 °C for 24 h. The dry cockle shell was then preheated at 200 °C to increase brittleness and simplify preliminary crushing into a coarse powder with an adapted crushing machine. The obtained coarse powder was milled for 1 h into a finer powder using a planetary ball mill (Fritsch GMBH, Pulverisette 6) with a silicon nitride (Si₃N₄) ball and jar at a rotation speed of 350 rpm. The milled powder was passed through a 325 mesh with a vibrating sieve machine (Nitto, ANF-30) to obtain particles of less than 45 µm. This powder was used as the calcium source for the synthesis of CT. Some of the milled and sieved cockle shell powder was then heated in air in a muffle furnace (Carbolite, RHF 16/8) at 900 °C for 2 h to transform CaCO₃ into CaO as a source of calcium for the synthesis of HAp. The calcined CaO powder was analyzed by XRD (Fig. 2). The minor phase of calcium hydroxide (Ca(OH)₂) present in the sample was due to the absorption of moisture from the air [30].

Preparation of reactant powders

Combustion synthesis of calcium titanate (CT) powder

Cockle shell powder with a particle size of 45 µm was mixed to homogeneity with anatase titanium dioxide powder (A-TiO₂, 99.5%, <45 µm, Degussa AG), by ball milling for 2 h using zirconia (ZrO₂) balls and a nylon bottle. The molar ratio of cockle shell powder to A-TiO₂ was 1.2: 1. In order to activate the solid-state reaction, the mixed powder was high-energy milled at 400 rpm for 30 min. The high-energy milled powder was then mixed at a molar ratio of 1:2 with magnesium powder fuel (Mg, 99%, ~45 µm, Riedel-Detlaen) by ball milling for 60 min. Using a hydraulic press (Huat

**Fig. 2** XRD pattern of cockle shell powder calcined at 900 °C

Seng, 1939-15 T), 20 g of the obtained reactant powder were uniaxially pressed at 5 psi (0.03 MPa) into a cylindrical steel mold with a diameter of 25.4 mm. To provide the high heat necessary for combustion, a 5 g thermite compact was prepared from iron oxide (Fe₂O₃, 99%, <5 µm, Sigma-Aldrich) and aluminium (Al, 93%, 45 µm, Himedia Laboratories) powders mixed at a molar ratio of 1: 2. The thermite compact was placed on top of the reactant compact and ignited. The combustion synthesis of CT took place under a controlled Ar atmosphere at a pressure of 0.5 MPa. The as-combusted product was separated from the by-product of thermite (Fe + Al₂O₃) and mechanically pestled into friable powder in an alumina (Al₂O₃) mortar. The by-product of magnesium oxide (MgO) was then leached from the powder product in 2 M hydrochloric acid (HCl, 37%, RCI Labscan) solution. Leaching was performed under moderate magnetic stirring for 180 min with a powder product-HCl solution ratio of 10 g: 100 mL. The as-leached sediment was captured with filter paper and washed several times with deionized (DI) water to neutralize pH. The washed as-leached powder was dried at 80 °C for 24 h and CT powder was obtained. The experimental procedures were adapted from and followed previous works [31, 32].

Precipitation of hydroxyapatite (HAp) powder

As-prepared CaO powder was suspended in DI water at a solid-liquid ratio of 20 g: 500 mL under constant magnetic stirring at 90 °C for 1 h. A suspension of 0.5 M Ca(OH)₂ was obtained with a pH of 13.0. The pH of the suspension was then adjusted to 7.0 with orthophosphoric acid (H₃PO₄, 85%, RCI Labscan) solution under constant stirring at 90 °C for 1 h. After cooling the mixture down to room temperature,

ammonium hydroxide (NH_4OH , 30%, J.T.Baker) solution was added to the suspension under stirring to achieve a pH of 10.0. The suspension was then aged for 48 h at room temperature in a covered beaker while precipitation occurred. The precipitated powder was recovered with a filter paper attached to a suction pump. The recovered powder was washed repeatedly with DI water to remove the NH_4^+ ion until pH was 7.0. The powder was then dried in an oven at 80 °C for 24 h, ground, and finally calcined in air at 700 °C for 2 h at a heating rate of 5 °C/min.

Conventional solid-state sintering of CT-HAp composites

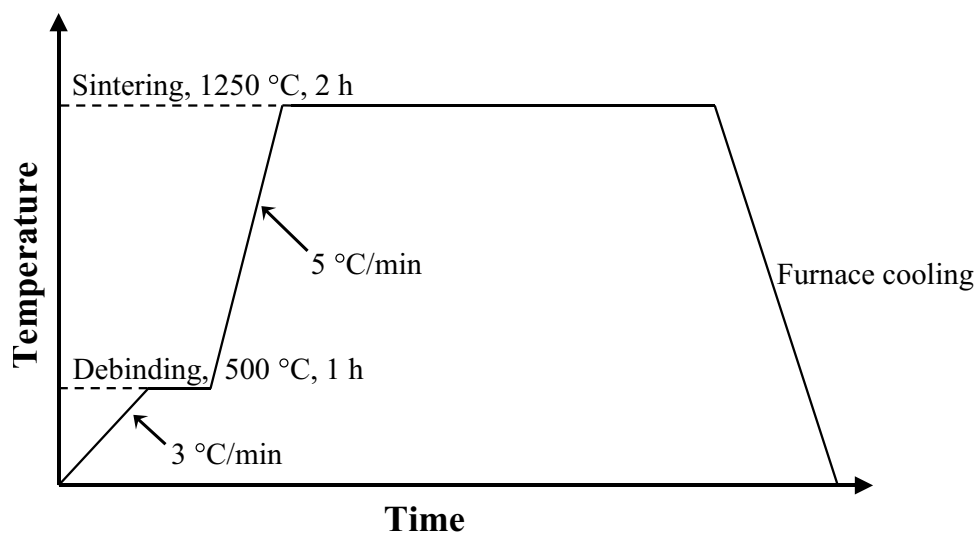
Various contents of CT powder (0–20%wt) were ball milled with HAp powder for 24 h in a wet medium (ethanol, 99.9%, RCI Labscan) using ZrO_2 milling balls. Wet milling was used to ensure a homogenous mixture of the two different ceramic powders. Ethanol was removed by drying the powder mixture in an oven at 80 °C. The dried powder was mechanically ground in an agate mortar and 0.5 g of the powder was mixed with 0.1 mL of 3 wt% polyvinyl alcohol (PVA, 99%, Gohsenol) solution. The obtained mixture was uniaxially pressed (Krumor, HP-900) at 50 MPa to form a disc-shaped green pellet 15 mm in diameter and approximately 1.5 mm thick. The green composite pellet was sintered by a conventional solid-state route in air in a muffle furnace (Carbolite, RHF 16/8). The PVA binder was eliminated by heating for 1 h at 500 °C, and the composite pellet was further heated at 5 °C/min to 1250 °C and held at this temperature for 2 h. Sintering at 1250 °C was reported in a previous study to produce HAp ceramics with acceptable properties and without any phase transformation into

tricalcium phosphate [33]. The sintering profile is depicted in Fig. 3.

Materials characterization

The chemical composition of raw cockle shell was analyzed using XRF (PANalytical, Zetium). Different phases in the raw materials, reactant powders and sintered composites were identified by XRD analysis (PANalytical, Empyrean), carried out using Cu-K_α radiation. The crystal structures of identified phases were analyzed and matched by HighScore Plus software version 4.7. The heavy metal content of raw cockle shell was determined by ICP-MS (PerkinElmer, NexION2000). The elements present in the SBF solution that was used to test chemical solubility were identified by inductively coupled plasma optical emission spectroscopy (ICP-OES, PerkinElmer, AVIO 500). Hg content in raw cockle shell was determined by direct mercury analysis (NIC, MA3000). A scanning electron microscope (SEM, FEI, Quanta 400) was used to study the morphology and measure the particle size of as-prepared CT and HAp powders and to observe the microstructure of sintered composites. The average grain size of sintered composite samples was measured from SEM images by the mean linear intercept method, using ImageJ software version 1.53e. Prior to SEM observation, samples were sputter-coated (SPI, 12157Q-AB) with a thin layer of gold to enhance electrical conductivity. The particle size of as-prepared HAp was precisely evaluated by transmission electron microscopy (TEM, JEOL, JSM-2010). Energy dispersive X-Ray spectroscopy (EDX, X-Max, Oxford) was used to analyze the elemental distribution in sintered composites and to measure the content of Ca and P in HAp.

Fig. 3 Temperature profile for the fabrication of CT-HAp composites by conventional solid-state sintering



Materials properties

Physical properties

Ceramic composites were then hydrostatically weighed with a precision analytical balance (Sartorius, B5A224S-CW). In accordance with the ASTM C373-72 standard, CT-HAp specimens were first soaked in boiling distilled water for 5 h and then left immersed in distilled water at room temperature for 8 h. The sintered density and apparent porosity of ceramic composites were calculated using Eqs. (1) and (2) [33]:

$$\rho_{\text{sintered}} (\text{g/cm}^3) = \frac{W_0}{W_2 - W_1} \times \rho_{\text{water}} \quad (1)$$

$$P_{\text{app}} (\%) = \frac{W_2 - W_0}{W_2 - W_1} \times 100\% \quad (2)$$

where ρ_{sintered} is the sintered density and P_{app} is the apparent porosity; W_0 , W_1 , and W_2 are the specimen dry weight, weight in water of the water-saturated specimen, and weight in air of the water-saturated specimen, respectively, and ρ_{water} is the density of water (1 g/cm³). The linear shrinkage of the ceramic composites was calculated using Eq. (3) [33]:

$$\text{Linear shrinkage} (\%) = \frac{D_b - D_a}{D_b} \times 100\% \quad (3)$$

where D_b and D_a denote the diameter of specimens before and after sintering.

Mechanical properties

The strength of CT-HAp composites was tested by determining biaxial flexure in accordance with the ISO/DIS 6872: 2013(E) standards, using a universal testing machine (Shimadzu, AGX-V). Disc-shaped specimens were prepared to the stipulated minimum thickness of 1.2 ± 2 mm and diameter of 12 mm. Specimens were placed on three hardened steel ball supports and the load was applied by a flat punch with a diameter of 1.5 mm at a crosshead speed of 0.5 mm/min. Biaxial flexural strength was calculated using Eq. (4) [33]:

$$\sigma (\text{MPa}) = -\frac{0.2387P(X - Y)}{b^2} \quad (4)$$

where σ is biaxial flexural strength, P is the load to failure and b is the specimen thickness at the fracture origin. X and Y were determined using the following formulas [33]:

$$X = (1 + \nu) \ln \left(\frac{r_2}{r_3} \right)^2 + \left[\frac{1 - \nu}{2} \right] \left(\frac{r_2}{r_3} \right)^2 \quad (4.1)$$

$$Y = (1 + \nu) \left[1 + \ln \left(\frac{r_1}{r_3} \right)^2 \right] + (1 - \nu) \left(\frac{r_1}{r_3} \right)^2 \quad (4.2)$$

where, ν is Poisson's ratio (0.25 for ceramic), r_1 is the radius of the support circle (1.6 mm), r_2 is the radius of the loaded area (0.8 mm) and r_3 is the radius of the specimen.

The hardness of samples was determined using the Vickers micro-hardness test (Innovatest, NOVA 130/240) by indenting a diamond pyramid tip on a smooth polished surface with a load of 1 kg_f (9.81 N) and dwell time of 10 s. The obtained Vickers hardness numbers were converted to GPa in SI units. In addition, the lengths of cracks emanating from the vertices of the diamond indentation were scaled by SEM and used to estimate the fracture toughness (K_{IC}) of specimens in radial-median and any other crack systems, using Eqs. (5) and (6) [34]:

$$K_{\text{IC}} (\text{MPa.m}^{1/2}) = 0.016 \times \frac{F}{c^{3/2}} \times \left(\frac{E}{\text{HV}} \right)^{1/2} \quad (5)$$

$$K_{\text{IC}} (\text{MPa.m}^{1/2}) = 0.0782 \times (\text{HV} \times a^{1/2}) \times \left(\frac{E}{\text{HV}} \right)^{2/5} \times \left(\frac{c}{a} \right)^{-1.56} \quad (6)$$

where, K_{IC} is fracture toughness, F is the applied load (N), E is Young's modulus (GPa), HV is Vickers hardness (GPa), c is the longest lateral extension of a crack from the centre of the indentation (m), and a is the half of the indentation diagonal (m). The Young's modulus (assumed $E \approx E_c$) of the particulate composite was estimated from the rule of mixture in Eq. (7) [35]:

$$E_c (\text{GPa}) = E_m V_m + E_p V_p \quad (7)$$

where, E_m and E_p denote the elastic modulus for the matrix (HAp = 79 GPa) and reinforcing material (CT = 161 GPa), respectively, and V_m and V_p denote the volume fractions of the matrix and reinforced particle, respectively.

Hardness and fracture toughness were used to determine the brittleness (B) of specimens, defined as [6]:

$$B (\mu\text{m}^{-1/2}) = \frac{\text{HV}}{K_{\text{IC}}} \quad (8)$$

Chemical solubility

The chemical solubility of the CT-HAp composites was investigated in a simulated human extracellular fluid using a solution of SBF. The SBF solution was prepared according to the method of Kokubo and Takadama [36] by mixing sodium chloride (NaCl, 7.996 g), sodium bicarbonate (NaHCO₃, 0.350 g), potassium chloride (KCl, 0.224 g), potassium biphosphate trihydrate (K₂HPO₄·3H₂O,

0.228 g), magnesium chloride hexahydrate ($\text{MgCl}_2 \cdot 6\text{H}_2\text{O}$, 0.305 g), calcium chloride (CaCl_2 , 0.278 g), sodium sulfate (Na_2SO_4 , 0.071 g), tris(hydroxymethyl)aminomethane ($(\text{CH}_2\text{OH})_3\text{CNH}_2$, 6.057 g), 1 M hydrochloric acid solution (HCl , 1.43 mL), and DI water. The pH of the SBF solution was adjusted to 7.2. Samples for analysis were soaked in 500 mL of SBF solution for 7, 15, 21, and 28 days at a controlled temperature of 37 °C in a universal oven (Mettler, UN 55 PA 115 V). After soaking, the pH of samples was measured with a pH meter (Thermo-Orion, A111). Samples were then washed thoroughly with DI water and dried in an oven at 60 °C for 24 h. The chemical solubility of the ceramic composites was estimated from the weight remaining [37], calculated based on the weight before (W_1) and after (W_2) soaking, using Eq. (9):

$$\text{Weight remaining (\%)} = \frac{W_2}{W_1} \times 100\% \quad (9)$$

Furthermore, Ca, P and Ti in the SBF solution were determined by ICP-OES and the chemical composition of sample surfaces was investigated by EDX analysis.

In-vitro biological properties

Cell culture MC3T3-E1 osteoblastic cells from the American Type Culture Collection (ATCC) were cultured in 75 cm² cell culture flasks containing alpha minimum essential medium (Alpha MEM, Gibco). A standard incubator (Eppendorf, Cellxpert) was operated at 37 °C with 5% CO₂ and 95% relative humidity. The Alpha MEM was supplemented with a solution of 10% fetal bovine serum (FBS), 100 I.U./mL penicillin and 100 µg/mL streptomycin. The medium was replaced every 2–3 days, until cell densification remained at 80–90% for 3 days.

WST-1 assay to measure cell viability The viability of cultured MC3T3-E1 cells was investigated on HAp and CT-HAp composite samples. Samples were placed in 24-well plates and cells were seeded (using Alpha MEM), as described in the previous subsection. After incubation, the medium was aspirated, composite samples were washed with phosphate buffered saline (PBS) solution, and 2 mL of 0.25% trypsin–EDTA solution were added to each well. The plates were then placed in the incubator for 5 min at 37 °C in 5% CO₂. After that, 10 mL of medium were twice added by pipette into a 50 mL test tube, and centrifuged for 5 min (TOMY, MDX-310). Four milliliters of medium were added. Then, 10 µL of cells were sampled, stained with trypan blue dye ($\text{C}_{34}\text{H}_{28}\text{N}_6\text{O}_{14}\text{S}_4$, Thermo Fisher Scientific) and micro-pipetted into a hemocytometer. Cytotoxicity was evaluated by counting viable cells under a phase contrast microscope

(Olympus, CKK53). The number of cells was determined using Eq. (10) [38]:

$$\text{Number of cells (cells/mL)} = \frac{\text{Average cell count}}{4} \times \text{Dilution factor} \times 10^4 \quad (10)$$

*Dilution factor is usually 2.

In addition, approximately 1.5×10^4 MC3T3E-1 cells, counted with the hemocytometer, were seeded on composite samples, which were then washed twice with 1 mL of PBS solution containing 500 µL of Alpha MEM. The cells in each well were treated with 50 µL of WST-1 solution and incubated for 2 h. The optical density (OD) or absorbance of the solution was measured at 450 nm using an automated microplate reader (BioTek, Epoch). The percentage of cell viability was calculated from Eq. (11) [39]:

$$\text{Cell viability (\%)} = \frac{\text{OD}_{450 \text{ sample}}}{\text{OD}_{450 \text{ control}}} \times 100\% \quad (11)$$

where, $\text{OD}_{450 \text{ sample}}$ is the optical density obtained in the presence of WST-1 and $\text{OD}_{450 \text{ control}}$ is the optical density obtained in the absence of WST-1, measured at 450 nm.

Osteogenic induction and alkaline phosphatase staining

MC3T3E-1 cells were seeded in wells of a 24-well plate at a density of 1.5×10^4 cells per sample and incubated for two days in a complete growth medium (CGM), which was supplemented with 0.1 µM dexamethasone (Sigma-Aldrich), 50 µM L-ascorbic acid (Sigma-Aldrich), and 10 mM β-glycerolphosphate disodium salt hydrate (Sigma-Aldrich). Subsequently, the cells were osteogenically induced for 24 h using osteogenic induction medium (ODM). The induced cells were then cultured in CGM for an additional seven days. Alkaline phosphatase (ALP) staining was performed as previously described [40]. Briefly, the cells were fixed with 70% ethanol for 30 min and stained with a 0.2% (v/v) solution of 5-bromo-4-chloro-3-indolyl phosphate (BCIP)/nitro blue tetrazolium (NBT) (Sigma-Aldrich). The intensity of ALP staining was assessed using a stereomicroscope (Nikon, SM2745T). The number of blue-stained pixels was analyzed as a ratio to the total sample surface area. The percentage changes in ALP activity was calculated by comparison to the sample without CT (0 wt%).

Cell fixation for SEM observation Osteoblastic cell growths on composite samples were washed with 0.1 M PBS solution, to remove soluble proteins in the medium. Cells were fixed with 2.5% glutaraldehyde ($\text{C}_5\text{H}_8\text{O}_2$, Sigma-Aldrich) diluted in 0.2 M PBS at room temperature for 1–2 h, and then washed 2–3 times with 0.1 M PBS solution for 1–2 min, then with distilled water for 1–2 min. Cells adhering to surfaces were dehydrated using a series of ethanol solutions

(50, 60, 70, 80 and 90%). Adhering cells were soaked twice in each concentration for 15 min and then for 30 min in 100% ethanol solution. Finally, dehydration was completed in a critical-point dryer (CPD, Toursimis, Autosamdri 931).

Results and discussion

Characteristics of as-prepared reactant powders for CT-HAp composites

The XRD pattern of CT powder (Fig. 4(a)) indicated a major phase of orthorhombic CaTiO_3 (space group: Pbnm) and a secondary phase of titanium dioxide (TiO_2) at a very low concentration. The XRD pattern of HAp powder (Fig. 4(b)) showed only a pure $\text{Ca}_5(\text{PO}_4)_3\text{OH}$ phase (space group: P63/m) with a hexagonal crystal system. The crystal system and crystalline parameters of CaTiO_3 and $\text{Ca}_5(\text{PO}_4)_3\text{OH}$ phases were referenced in the powder diffraction file databases (according to the referenced PDF numbers).

The SEM image of CT powder (Fig. 5(a)) revealed irregular agglomerations with a particle size of less than 1 μm . The HAp powder (Fig. 5(b)) comprised clusters of small particles. TEM observation confirmed HAp particles were rod-like with a particle size in the nanometer range (Fig. 5(c) and (d)). The Ca/P ratio of hydroxyapatite used in this work, determined by EDX, was close to the Ca/P ratio of adult human bone (1.71) [41].

Characteristics and properties of conventional-sintered CT-HAp composites

HAp and CT-HAp composite samples, sintered at 1250 $^\circ\text{C}$ for 2 h, were analyzed using XRD. The XRD pattern of the

HAp sample (0%wt) (Fig. 6) presented single peaks of HAp with the chemical formula $\text{Ca}_5(\text{PO}_4)_3\text{OH}$. The XRD patterns of CT-HAp composites (2–20%wt of CT) presented major peaks of HAp and minor peaks of CT. The intensity of the CT peaks ($\sim 47.5^\circ$) increased with increments of CT content. These findings confirmed that HAp and CT-HAp composites had been synthesized without any phase dissociation or new phase formation. Unreacted TiO_2 , originally present in CT powder (Fig. 4(a)), was presented in very low amounts compared with HAp and CT, and therefore the peak of TiO_2 was not recorded.

SEM images of HAp and CT-HAp composites showed that the surface microstructure of all specimens (Fig. 7) comprised a bimodal grain size distribution of HAp particles smaller than 2 μm . The microstructures were homogenous and CT particles were evenly distributed in the HAp matrix at CT contents of 2 to 8%wt. In addition, the average grain size of the CT-HAp composites decreased from 1.14 ± 0.20 to 0.90 ± 0.06 μm with increments of CT content from 2 to 8%wt. The reduction of grain size was due to the effective inhibition of grain boundaries by CT particles. At 10%wt of CT and above, the microstructure of the CT-HAp composites became less homogenous, developing many pores, including large pores, and CT particles tended to agglomerate more and adhere to HAp. Also, more abnormal grain growth was observed and the average grain size increased from 0.98 ± 0.10 to 1.44 ± 0.35 μm as CT contents increased from 10 to 20%wt.

In addition, SEM images of cross-sections of HAp and the composites (Fig. 8) showed that composites with higher CT contents, in addition to increasing agglomeration of CT particles, exhibited greater porosity, displaying pores clustered around agglomerated particles of CT. Dubey et al. [6] in a study of CT-HAp composites containing high amounts

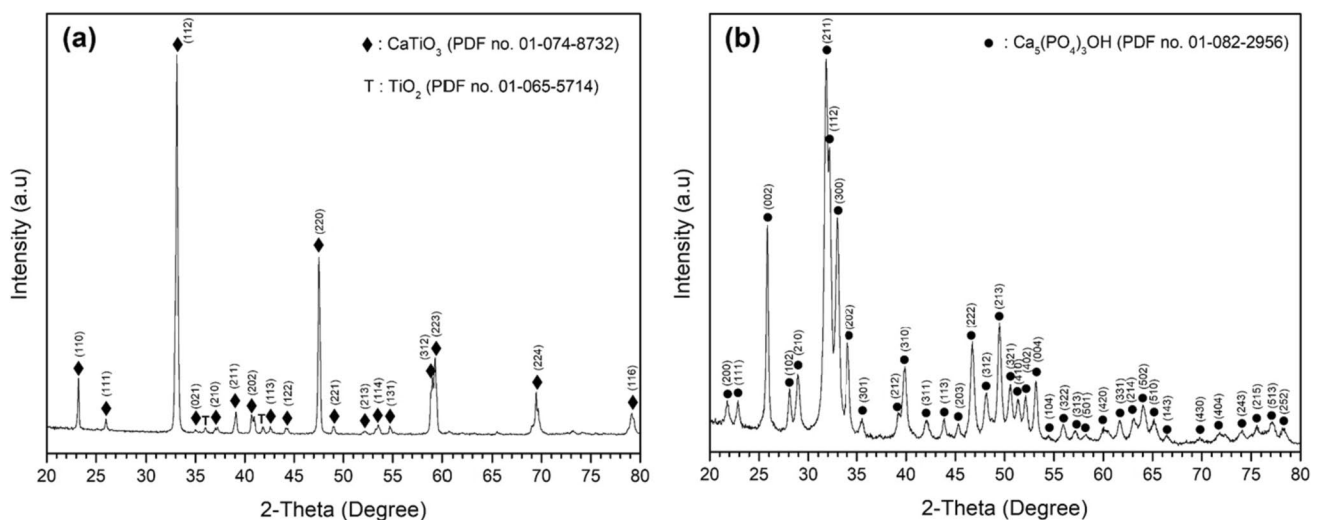


Fig. 4 XRD pattern of reactant powders (a) calcium titanate and (b) hydroxyapatite

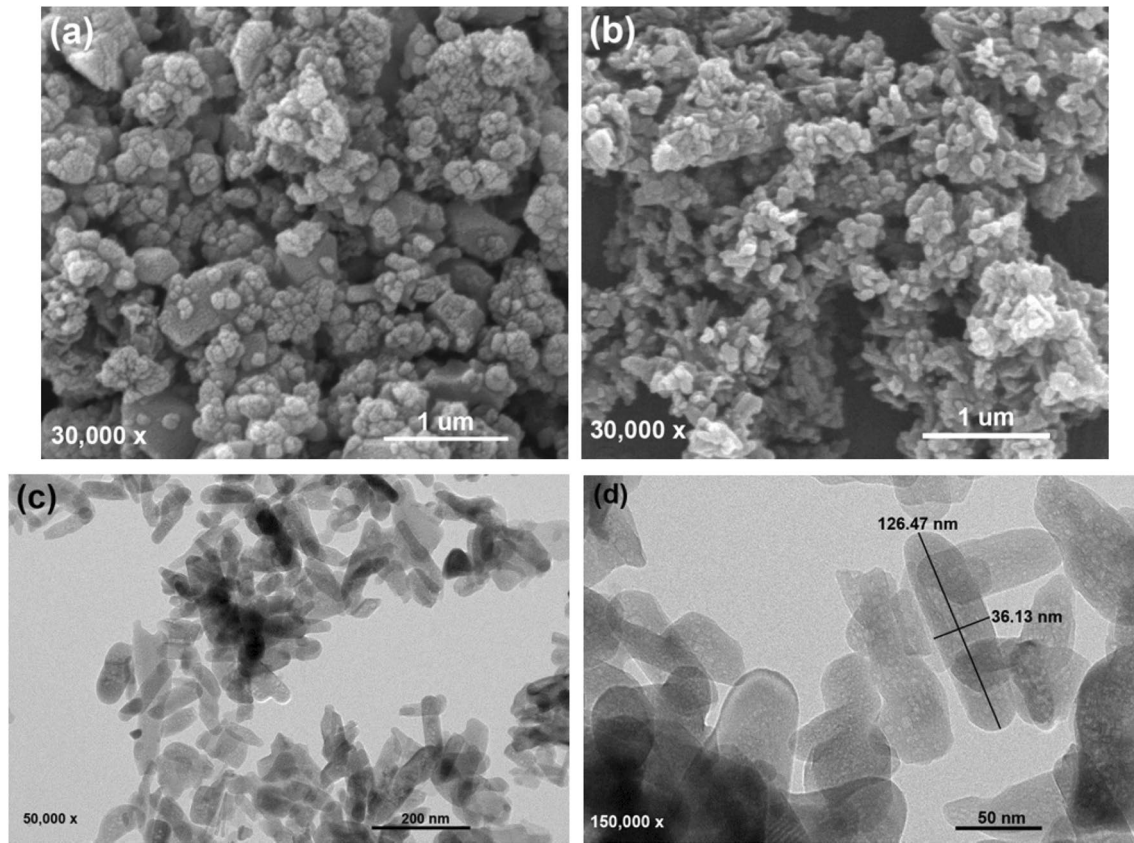


Fig. 5 The micrographs show SEM images of calcium titanate (a) and hydroxyapatite (b), and TEM images (c) and (d) of hydroxyapatite particles at different magnifications

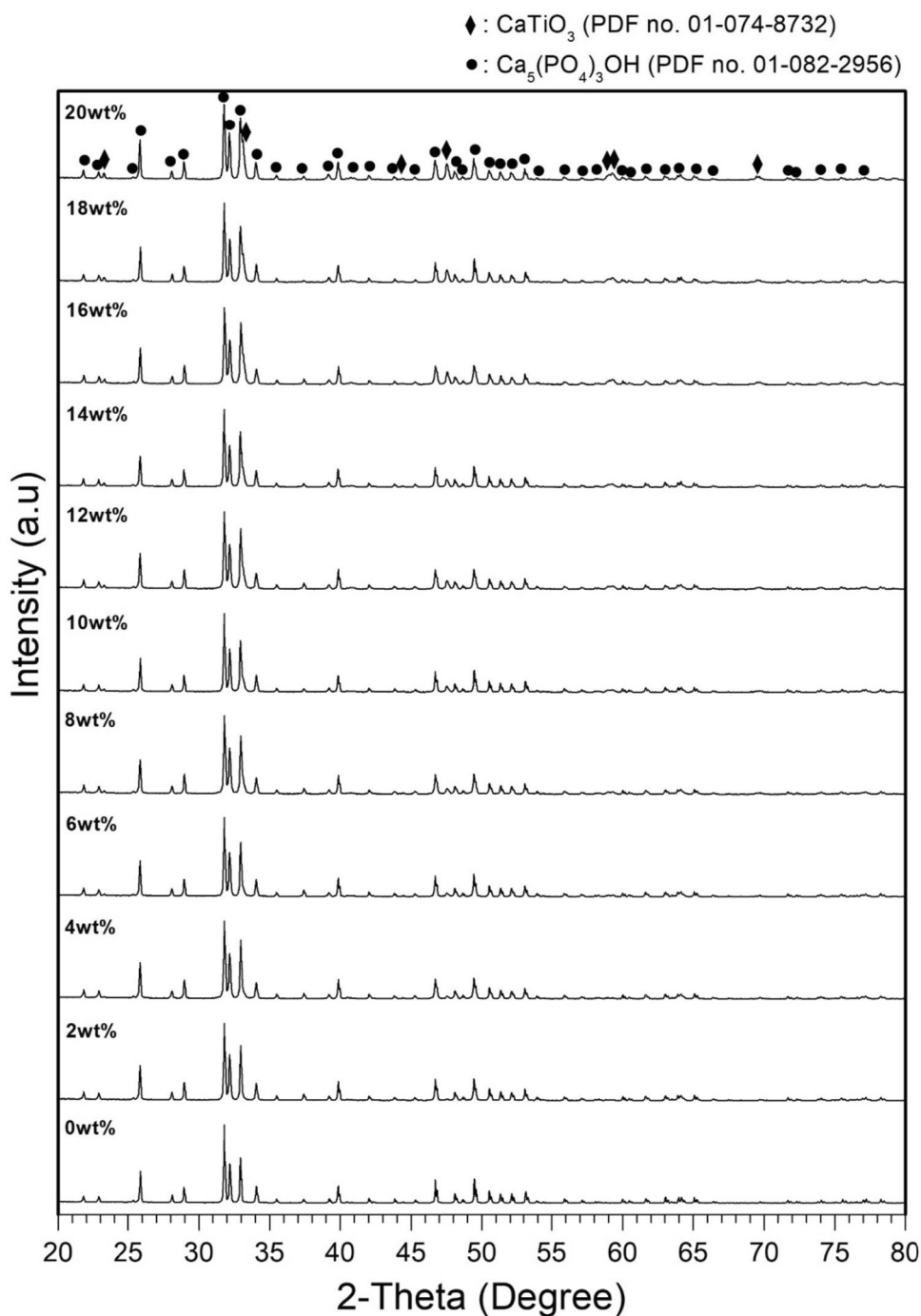
of CT, reported that the number of CT/CT contacts increased with increments of CT content. In the present work, CT-HAP composites containing more than 8%wt of CT exhibited increased agglomerations of CT. Also, this result might be affected by contacts between CT particles. In another work [1] more clusters of CT particles were observed at high CT contents.

To identify phase distributions, SEM-EDX elemental mapping was performed of HAp, CT and CT-HAP composites containing 10 and 20%wt of CT. HAp presented Ca, P and O (Fig. 9(a)), while CT and both CT-HAP composites presented Ca, P, Ti and O (Fig. 9(b) and (c)). CT has a higher density than HAp, and thus was visible as a brighter area. To confirm the findings, two different areas on the surface of CT-HAP with 20%wt of CT were scanned and EDX spectra were recorded (Fig. 9(d)). The darker area (marked *) presented Ca, O, and P with a small amount of Ti, indicating hydroxyapatite as the major phase. In contrast, the brighter area (marked ●) revealed the presence of Ca, Ti and O contents of 22.82, 20.84 and 56.34 at%, respectively, which were close to the relevant references [42] shown in the enclosed table. This result indicated that the composition of the brighter area of the composite was CT.

Physical and mechanical properties of conventional-sintered CT-HAP composites

The sintered density and apparent porosity of the synthesized materials were plotted as functions of CT content (Fig. 10). The density of HAp in this work was $2.97 \pm 0.08 \text{ g/cm}^3$ (94% of theoretical density). The density of CT-HAP composites with less than 8%wt of CT slightly increased as a function of CT content from 2.98 at 0wt% to $3.01 \pm 0.02 \text{ g/cm}^3$ at 6%wt of CT. The increasing density of CT-HAP composites with less than 8%wt of CT was in agreement with the rule of mixture for composites and the greater theoretical density of CT (3.98 g/cm^3) than HA (3.16 g/cm^3) [1, 35] but the density of 8%wt CT-HAP was very slightly lower at $3.00 \pm 0.01 \text{ g/cm}^3$. Above 8%wt of CT, the density of the composite slightly decreased, reaching its lowest value of $2.91 \pm 0.02 \text{ g/cm}^3$ at 20%wt of CT. The reduced density of the composite at CT contents of 8wt% and above was related to the increased porosity of the material. CT was denser than HAp, therefore, when CT particles were added to HAp powder in the consolidation process, the compressibility of the green sample was reduced and the porosity of the obtained CT-HAP composites increased as a function of CT content.

Fig. 6 XRD patterns of hydroxyapatite and calcium titanate-hydroxyapatite composites at different calcium titanate contents



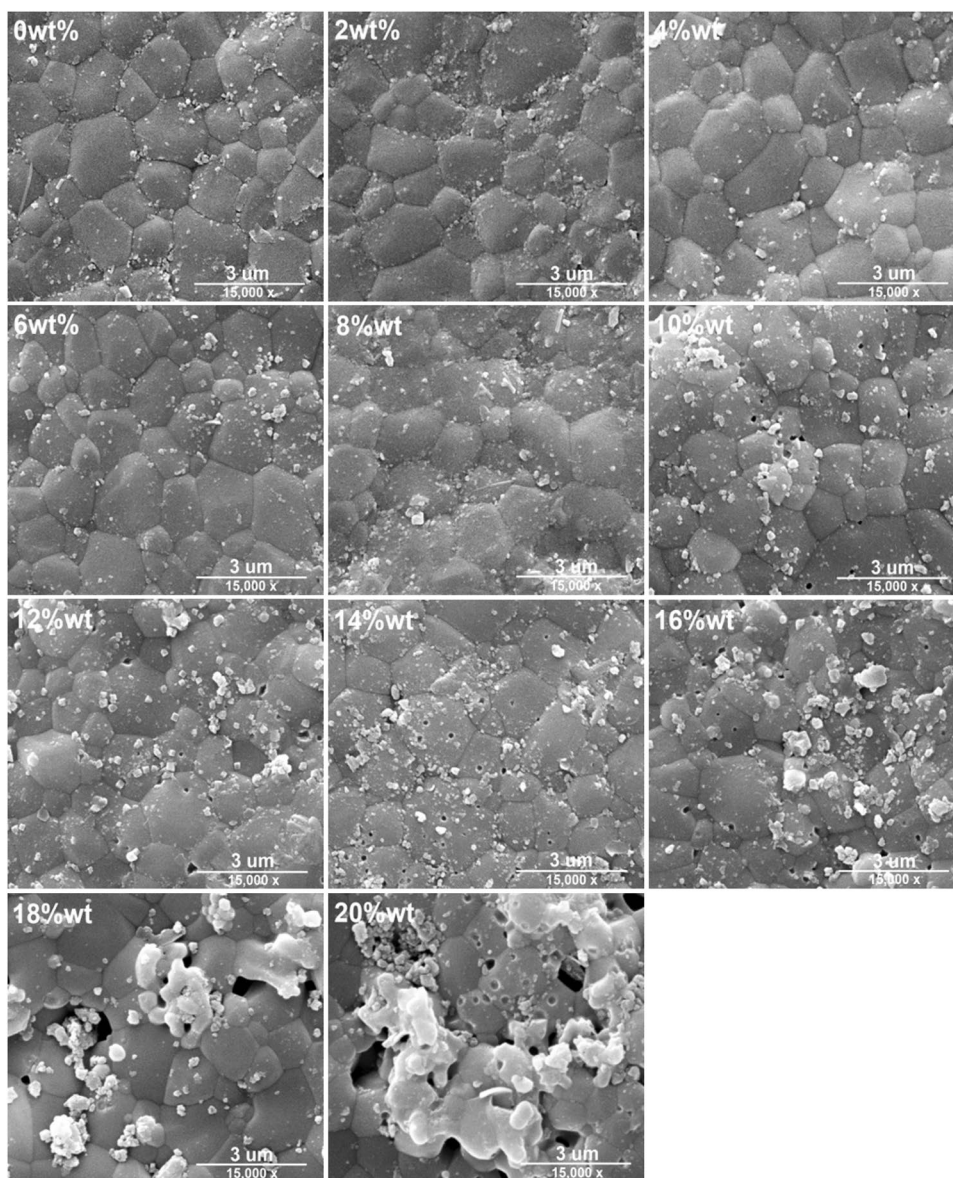
Also, the higher melting point of CT particles ($> 1900\text{ }^{\circ}\text{C}$ for CT and $\approx 1500\text{--}1600\text{ }^{\circ}\text{C}$ for HAp) [42–44], higher sintering temperature ($1450\text{ }^{\circ}\text{C}$) [3] and great resistance to deformation ($E = 161\text{ MPa}$) [45] inhibited microstructural rearrangement during sintering. The reduced deformation and diffusion of the particles further promoted porosity, and higher contents of CT possibly increased the porosity of the composite due to the more uniform grain growth.

The linear shrinkage of samples (Fig. 11) decreased with increments of CT content. The reduction in shrinkage of

the composite was mainly due to the non-densifying inclusion, namely CT, introduced into the HAp matrix. When the amount of CT in the composite was high, the contact between CT particles was excessive and led to the development of pores that hindered densification [6–8].

The biaxial flexural strength of the CT-HAp composite was affected by CT content. At CT contents from 2 to 8%wt, the flexural strength of the composite increased (Fig. 12). The flexural strength of 8%wt CT-HAp was $56.67 \pm 1.12\text{ MPa}$, compared to $45.56 \pm 2.71\text{ MPa}$ for pure HAp—an increase of

Fig. 7 SEM images of the surface morphology of hydroxyapatite and calcium titanate-hydroxyapatite composites at different calcium titanate contents



24%. In contrast, flexural strength decreased at CT contents from 10 to 20%wt. CT has greater flexural strength than HAp [7, 8] and therefore, CT-HAp composites with an optimal microstructure and specific mechanical and physical properties can be achieved by controlling the CT content. In the discussion of microstructural evolution in “[Characteristics of as-prepared reactant powders for CT-HAp composites](#)” section, the grain size, porosity, pore size and pore distribution were related to CT content (Figs. 7 and 8). Composites containing 8%wt of CT or less displayed smaller grain sizes than composites containing 10%wt of CT or more, as well as lower porosity and smaller pores that were more homogeneously distributed in the HAp matrix.

Figure 13 shows the microhardness of HAp and the CT-HAp composites. The hardness of the composite increased with increments of CT content from 2 to 8%wt. The 8%wtCT-HAp composite exhibited the greatest hardness and the microhardness of composites with 10wt% or more of CT was considerably lower, showing a similar trend to flexural strength (Fig. 12). The results indicated that the mechanical properties of the CT-HAp composite (including hardness) depended on the CT content. Ramírez et al., [45] suggested that the formation of hard CT particles ($HV \approx 5$ GPa) supported the reduction of HAp deformation. The hardness of the composite, like its flexural strength, was significantly impacted by porosity.

Fig. 8 SEM cross-sectional images of hydroxyapatite and calcium titanate-hydroxyapatite composites at different calcium titanate contents

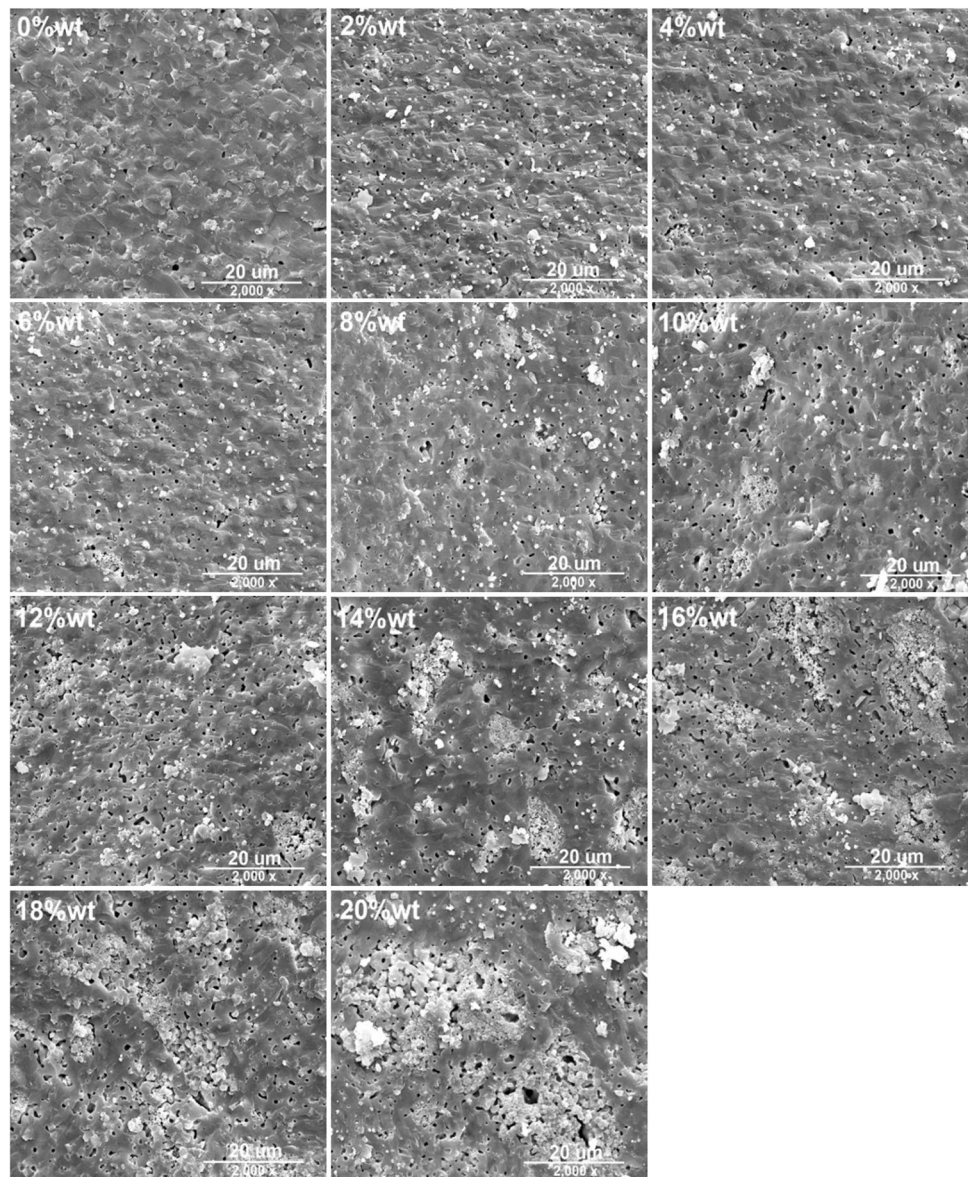
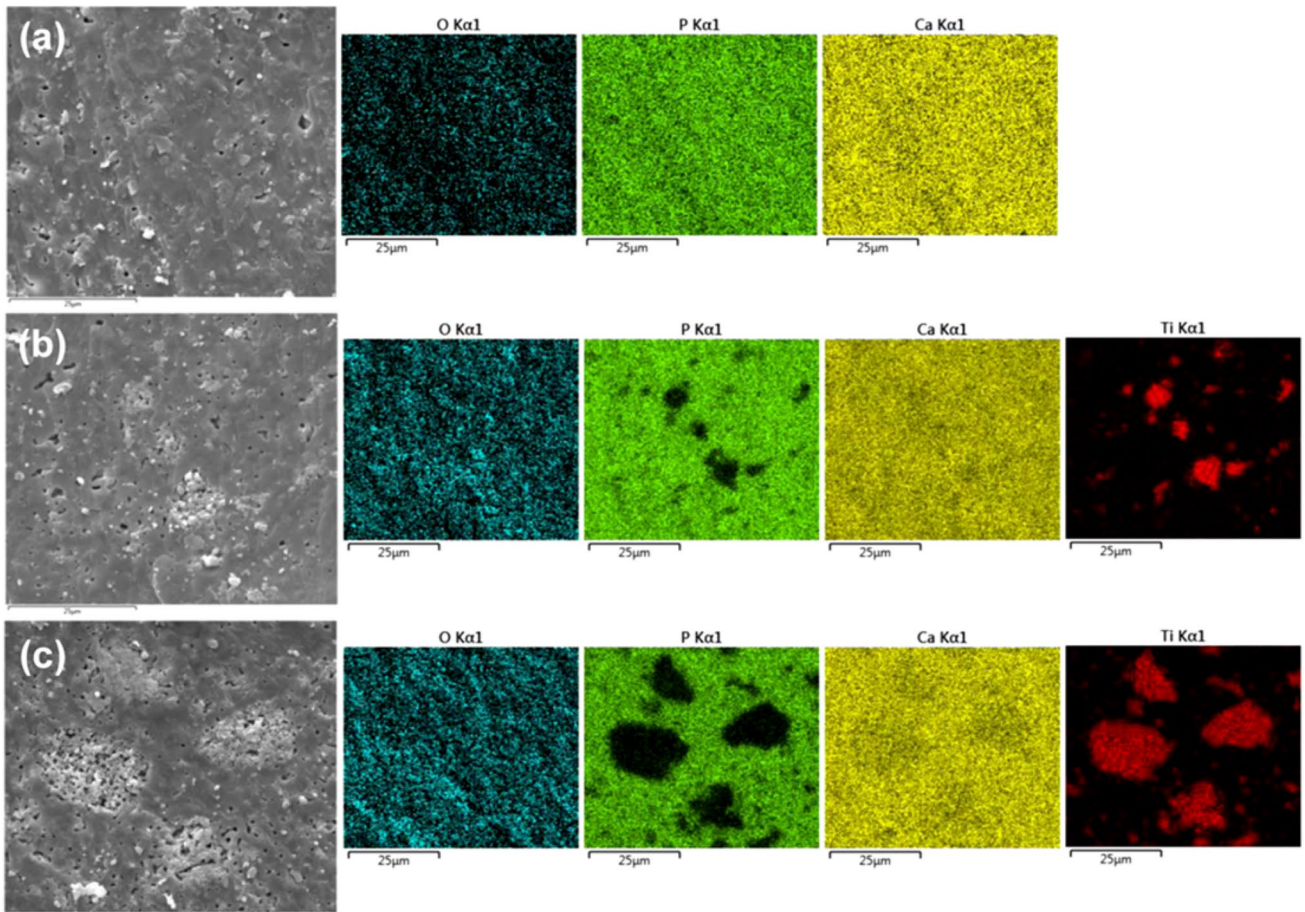


Figure 14(a) shows a sketch of a radial-medial crack and the imprint of the diamond tip on the specimen surface after Vickers hardness testing. SEM images (Fig. 14(b)–(e)) show the impact areas on HAp and CT-HAp composite samples after Vickers hardness testing. The images on the right-hand side are at higher magnification and show the opening of the crack after unloading. The cracks formed on the surface of pure HAp and 2 and 8%wtCT-HAp (Fig. 14(b)–(d)) were of the radial-medial type. The cracks diffused along the specimen surface, and the Vickers indent also caused regions of plastic deformation due to residual stresses at the point of the indent [46, 47]. However, no crack system could be clearly identified on the 20%wtCT-HAp composite (Fig. 14(e)), and the

residual imprint was larger than the imprint in the other composites. The SEM micrograph of the indented surface of the pure HAp sample (Fig. 14(b)) shows a mainly transgranular mechanism of fracture, but the fracture mechanism observed in all the composites (Fig. 14(c)–(e)) was less transgranular and the crack openings were narrower. The 2 and 8%wtCT-HAp composites exhibited greater fracture toughness (K_{IC}) than the HAp sample, with values of 5.75 and 7.77 $\text{MPa}\cdot\text{m}^{1/2}$, respectively, compared to 4.66 $\text{MPa}\cdot\text{m}^{1/2}$. This enhanced toughness contributed to the resistance to crack-growth of the composites. Moreover, to confirm the resistance to cracking, the brittleness (B) of the materials was determined by considering hardness and K_{IC} . The calculated B values of HAp and 2 and 8%wtCT-HAp



(d)

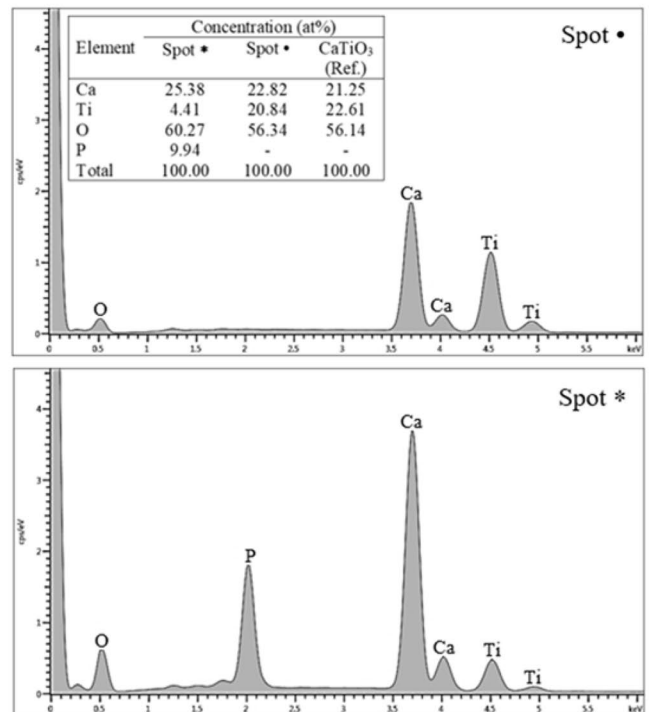
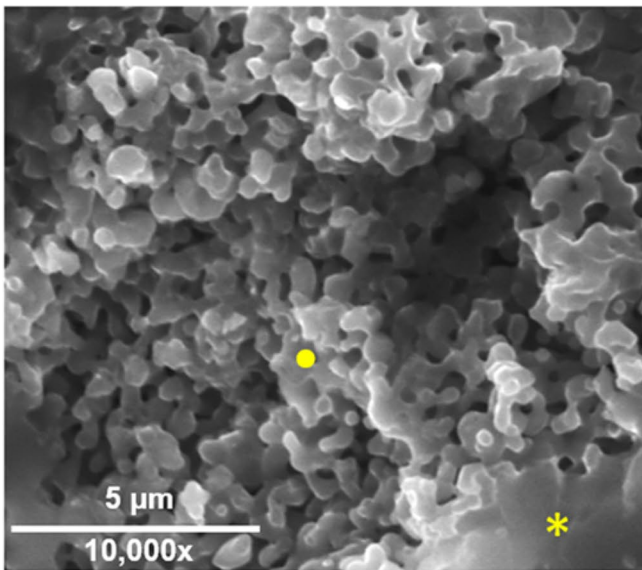


Fig. 9 Typical SEM-EDX mapping of hydroxyapatite (a) 0%wt calcium titanate, and calcium titanate-hydroxyapatite composites with calcium titanate contents of (b) 10%wt and (c) 20%wt, and (d) magnified SEM-EDX point scan of a calcium titanate-hydroxyapatite composite with 20%wt of calcium titanate

composites were 0.94, 0.88 and 0.75 $\mu\text{m}^{-1/2}$, respectively. According to a previous study [48], ceramics with low B and high K_{IC} values were less brittle because the concentration of stresses was insufficient to cause cracking. The 8%wt-CT-HAp sample demonstrated the largest K_{IC} . Crack

Fig. 10 Sintered density and apparent porosity of hydroxyapatite and calcium titanate-hydroxyapatite composites at different calcium titanate contents

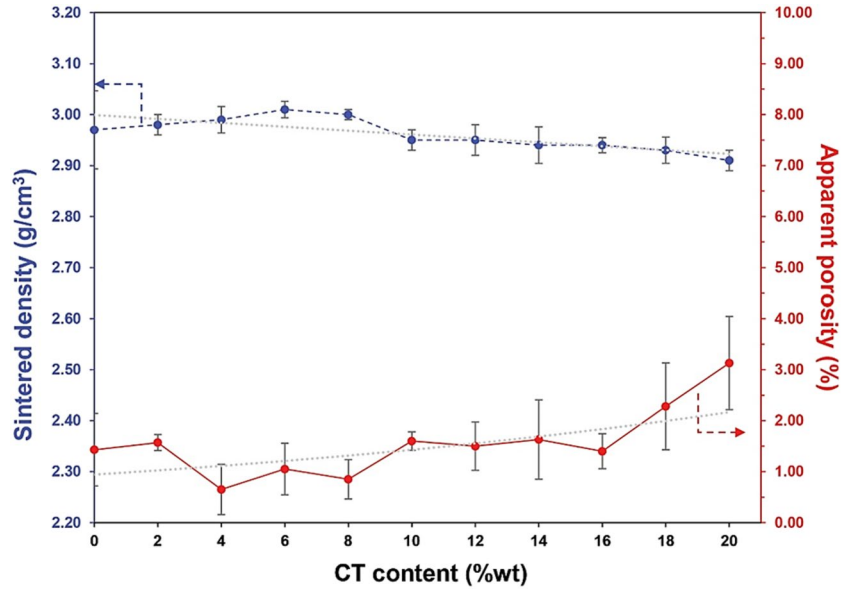


Fig. 11 Linear shrinkage of hydroxyapatite and calcium titanate-hydroxyapatite composites at different calcium titanate contents

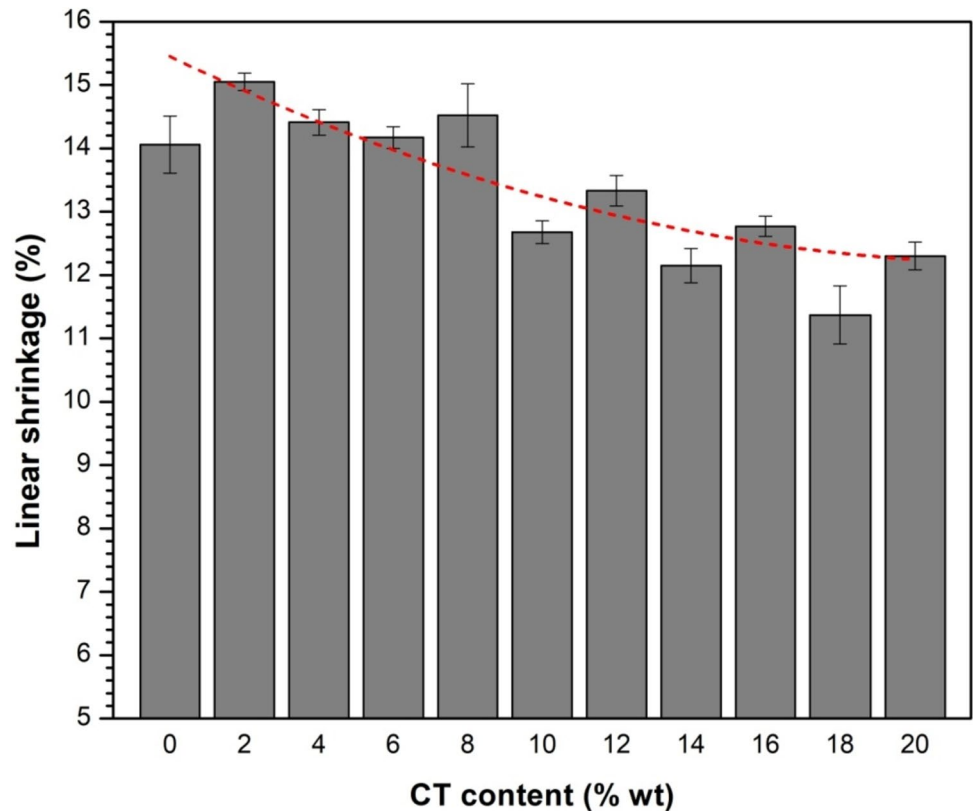
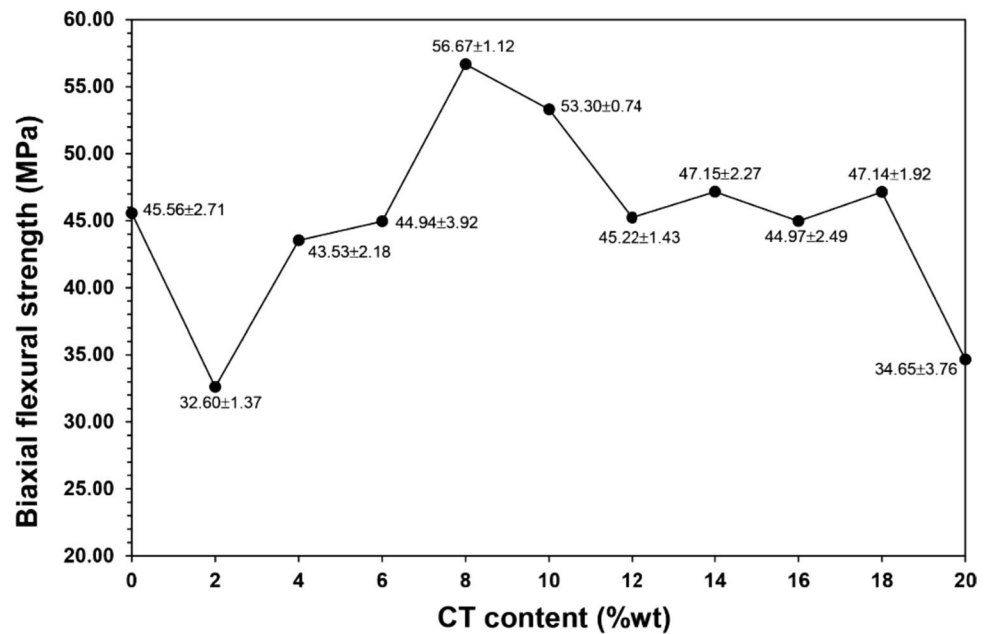


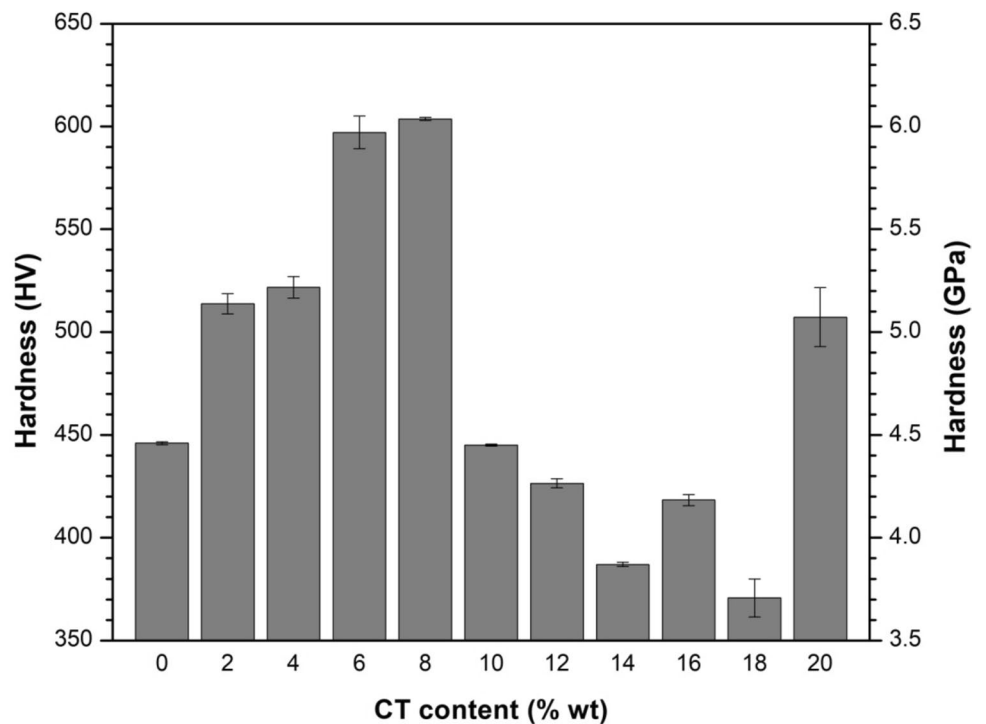
Fig. 12 Biaxial fractural strength of hydroxyapatite and calcium titanate-hydroxyapatite composites at different calcium titanate contents



propagation in this composite was restricted by homogeneously dispersed CT agglomerations in the HAp matrix, while the crack opening was very narrow (Fig. 15). This finding was consistent with the finding of J.G. Miranda-Hernandez et al. [49], who reported that fracture toughness

was increased by the presence of CT. On the other hand, the 20%wt-CT-HAp sample had a lower K_{IC} ($2.11 \text{ MPa} \cdot \text{m}^{1/2}$) and higher B ($2.35 \mu\text{m}^{-1/2}$) than the other samples. These poor properties were attributed to high porosity, low hardness and uneven distribution of CT particles.

Fig. 13 The microhardness of hydroxyapatite and calcium titanate-hydroxyapatite composites at different calcium titanate contents



Chemical solubility of CT-HAp composites

Figure 16 shows the weight remaining of HAp and CT-HAp composites soaked in SBF solution for various time periods. It can be seen from Fig. 16 that weight was not lost in a consistent pattern. After 28 days in SBF solution, the remaining weight of some samples was $99.97 \pm 0.11\%$ of the initial weight. The very low weight loss ($< 0.50\%$) of the samples was due to the high crystallinity and strong negative surface potential produced by sintering [50]. Also, the hexagonal HAp obtained in this work is highly stable in biological environments. The results indicated that CT-HAp composites degrade slowly and may be best used to repair bone defects which need a slow degradation rate. However, certain samples, 8%wt CT-HAp, for example, showed a greater average weight loss than others in the case of 8%wt CT-HAp, 0.32% compared to 0.08–0.20%. It is possible that the as-sintered sample set contained more surface defects such as micro-cracks, small pores and roughness [51, 52], which increased solubility by increasing the area exposed to SBF [53, 54].

Table 3 shows concentrations of Ca^{2+} and PO_4^{3-} ions found in SBF solution after soaking HAp and CT-HAp samples for various time periods. The Ti^{4+} ion was not detected in any condition. It can be seen that concentrations of Ca^{2+} and PO_4^{3-} ions were lower after 7 days of soaking compared to the concentration of both ions found in fresh SBF. Concentrations were higher at 15 days and higher still at 21 days, increasing from 67.75 ± 1.13 to 78.51 ± 0.28 ppm for Ca^{2+} , and from 51.82 ± 1.21 to 59.15 ± 0.09 for PO_4^{3-} . Concentrations of both ions were lower at 28 days than at 21 days since the ions precipitated onto the samples. Indeed, the dissolution of Ca^{2+} from the CT-HAp composite promoted the exchange of ions on its surface. The exchange between Ca^{2+} ion from the composite and PO_4^{3-} ion from the SBF solution induced the surface precipitation of apatite [50, 55, 56].

The elemental compositions of sample surfaces after soaking in SBF solution were determined by EDX analysis. The results showed that Ca and P concentrations and the Ca/P ratio on sample surfaces tended to increase with soaking time (Table 4). However, little fluctuation was noticed in the case of Ti. The increases in Ca and P concentrations were mainly attributed to the precipitation of titanate (TiO_3^{2-}) and phosphate to form apatite by a dissolution-precipitation reaction [57, 58]. When the samples were soaked in SBF solution, the negatively charged OH^- and HPO_4^{2-} ions combined with positively charged Ca^{2+} ions to form Ca-rich calcium phosphate. With the accumulation of Ca ions, the surfaces were positively charged, and PO_4^{3-} ions could easily attach [59]. The Ca/P ratio was up to 2.26 times higher than the theoretical value (1.67) of HAp due to the initial high Ca

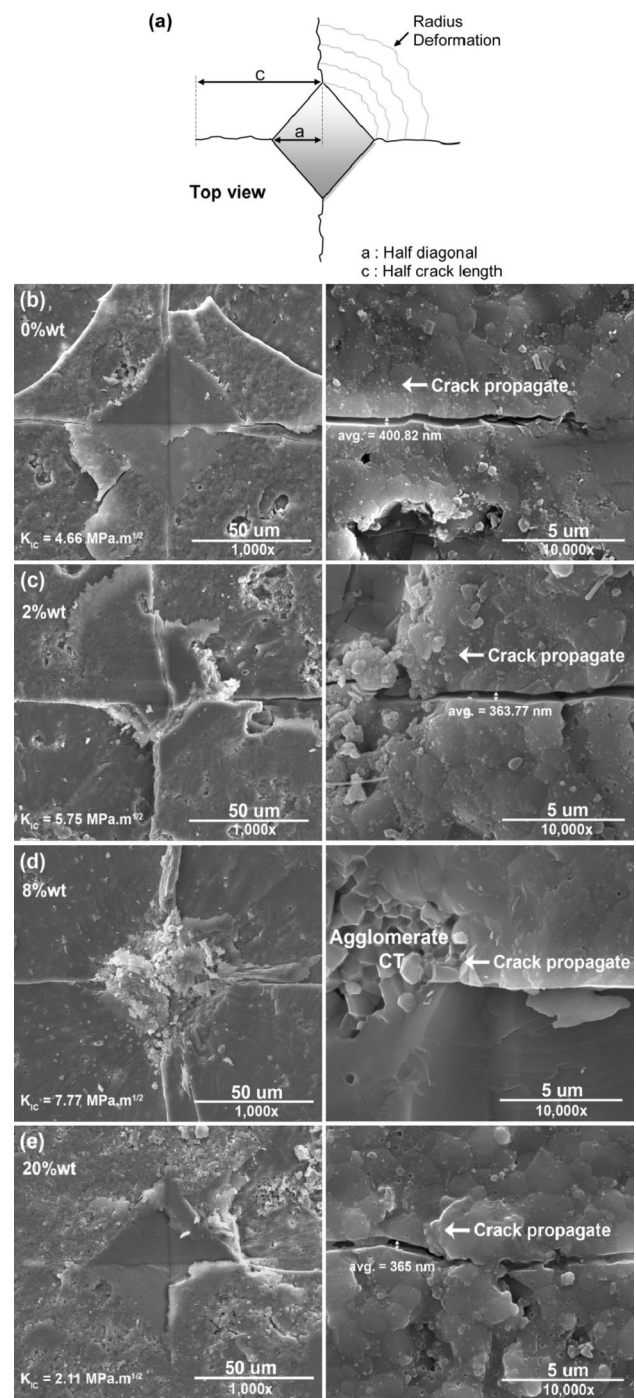
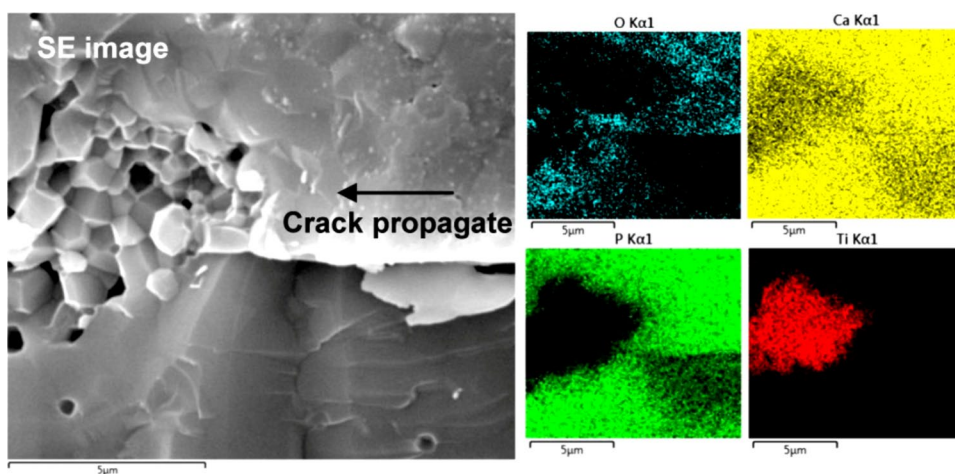


Fig. 14 The sketch (a) shows the imprint of the diamond tip and a radial-median crack formed after hardness testing. Images (b), (c), (d), and (e) show residual imprints (left) with crack openings (right) of hydroxyapatite and calcium titanate-hydroxyapatite composites with calcium titanate contents of 2, 8 and 20%wt

concentration in both CT and HAp. Furthermore, the large Ca content was ascribed to the initial adsorption of Ca ions from CaCl_2 in SBF solution through ionic interaction with negatively charged phosphate groups. The high Ca/P ratio

Fig. 15 SEM-EDX mapping of calcium titanate-hydroxyapatite composite with 8%wt of calcium titanate



on the sample surface was a result of bioactivity that was proposed as a positive development [60]. In addition, minor elements such as Mg, Na, Cl and K, were found on the specimen surface in some conditions. These elements were present in the fresh SBF solution and could precipitate on sample surfaces as $\text{Mg}(\text{OH})_2$ and NaCl [61, 62].

Dubey et al. [4] proposed that bone formation on the negatively charged surface of HAp (negative hydroxyl and phosphate groups) [11] was enhanced by osteoconductivity and that the accumulation of positively charged Ca^{2+} ions depended on electrical conductivity. Other studies of CT-HAp composites [7, 63] reported that the higher electrical conductivity of CT particles (3.2×10^{-5} S/m compared to 2.4×10^{-16} S/m for HAp) enhanced the electrical conductivity of the composite. The enhancement

of electrical conductivity has been attributed to ionic polarization caused by the displacement between Ti^{3+} and O^{2-} in CT [4] and supports the osseointegration and osteoconductivity of bone tissue. Therefore, CT-HAp composites that contain the optimal CT content can promote electrical conductivity to generate better bioactive properties than are exhibited by pure HAp.

In-vitro biological properties of CT-HAp composites

WST-1 assay results were obtained after growing MC3T3-E1 osteoblast cells on CT-HAp composites for three days. The 8%wtCT-HAp composite produced the highest cell viability (Fig. 17). Perhaps the microstructure of this composite was more compatible for cellular

Fig. 16 The weight remaining of hydroxyapatite and calcium titanate-hydroxyapatite composites at different calcium titanate contents soaked in SBF solution for different time periods

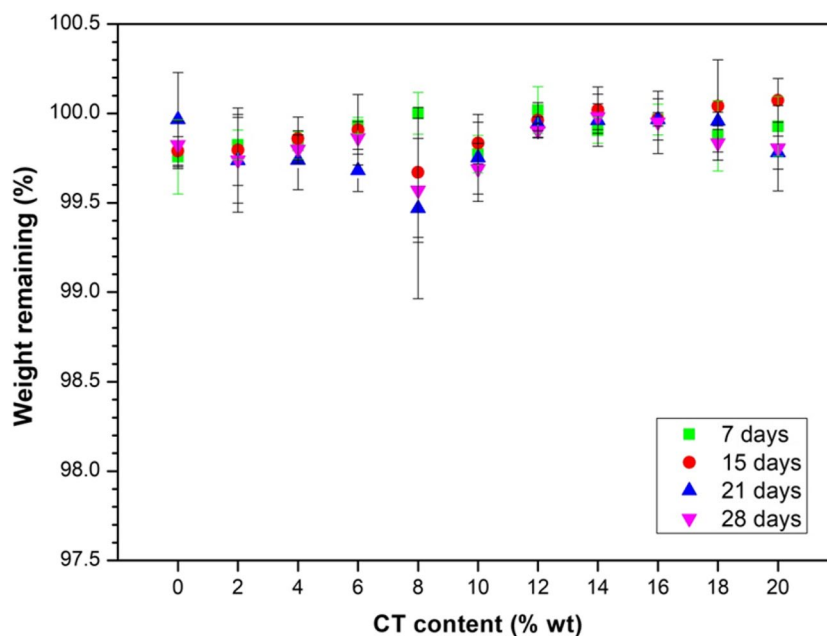


Table 3 The ions released from calcium titanate-hydroxyapatite composites into simulated body fluid solution after soaking for different time periods were detected by ICP-OES

Soaking period (Day)	Ion and concentration (ppm)			pH
	Ca ²⁺	PO ₄ ³⁻	Ti ⁴⁺	
Fresh SBF	85.21 ± 1.63	65.80 ± 0.19	Not found	7.20
7	64.50 ± 1.29	50.11 ± 0.40	Not found	7.11
15	67.75 ± 1.13	51.82 ± 1.21	Not found	7.16
21	78.51 ± 0.28	59.15 ± 0.09	Not found	7.17
28	75.73 ± 1.43	57.53 ± 0.52	Not found	7.16

survival. SEM observation of 8%wtCT-HAp revealed a better distribution of CT particles in the HAp matrix. Other factors also influenced cell viability. The grain size and porosity of the composites were involved. The

8%wtCT-HAp composite had a small grain size and low porosity compared to 10–20%wtCT-HAp composites. Contact between the osteoblastic cells and the material surface was better and the levels of calcium and phosphate ions for apatite formation were higher [11, 12]. Moreover, the surface roughness of the material was correlated with the enhancement of polar components and cell attachment [64]. The surface morphology of 8%wtCT-HAp was perhaps more suitable for cell adherence and therefore cell survival.

SEM images of osteoblast cells cultured on the sintered materials showed that all CT-HAp composites and pure HAp (0% wt) exhibited good cell attachment, without any sign of cytotoxicity. With increments of CT content up to 6%wt, cells were elongated and attached with long filopodia (Fig. 18). At CT contents from 8 to 20%wt,

Table 4 Elements detected on the surface of the calcium titanate-hydroxyapatite composites after soaking in SBF solution for different time periods

Soaking period (Day)	Element and concentration (%wt)									
	Ca	P	Ca/P	Ti	O	Mg	Na	Cl	K	
Unsoaked	25.91 ± 0.49	14.70 ± 0.26	1.76	1.26 ± 0.02	58.13 ± 0.69	Undetected	Undetected	Undetected	Undetected	
7	35.59 ± 0.41	15.82 ± 0.78	2.25	1.08 ± 0.02	43.29 ± 0.18	0.13 ± 0.05	Undetected	Undetected	Undetected	
15	37.39 ± 0.19	17.26 ± 0.12	2.17	2.69 ± 1.04	44.79 ± 0.13	0.71 ± 0.26	0.21 ± 0.03	0.12 ± 0.03	0.08 ± 0.04	
21	38.85 ± 0.39	17.22 ± 0.41	2.26	1.38 ± 0.08	42.36 ± 0.72	0.18 ± 0.03	Undetected	Undetected	Undetected	
28	38.34 ± 0.34	17.15 ± 0.21	2.23	1.29 ± 0.08	43.38 ± 0.21	0.10 ± 0.01	Undetected	Undetected	Undetected	

Fig. 17 Cell viability of MC3T3-E1 osteoblast cells after three days growing on hydroxyapatite and calcium titanate-hydroxyapatite composites with different calcium titanate contents. Results were analyzed by a one-way ANOVA and Scheffe's post-hoc test. *P* values < 0.05 were considered statistically significant. *denotes a statistically significant difference with respect to control (0%wt of calcium titanate)

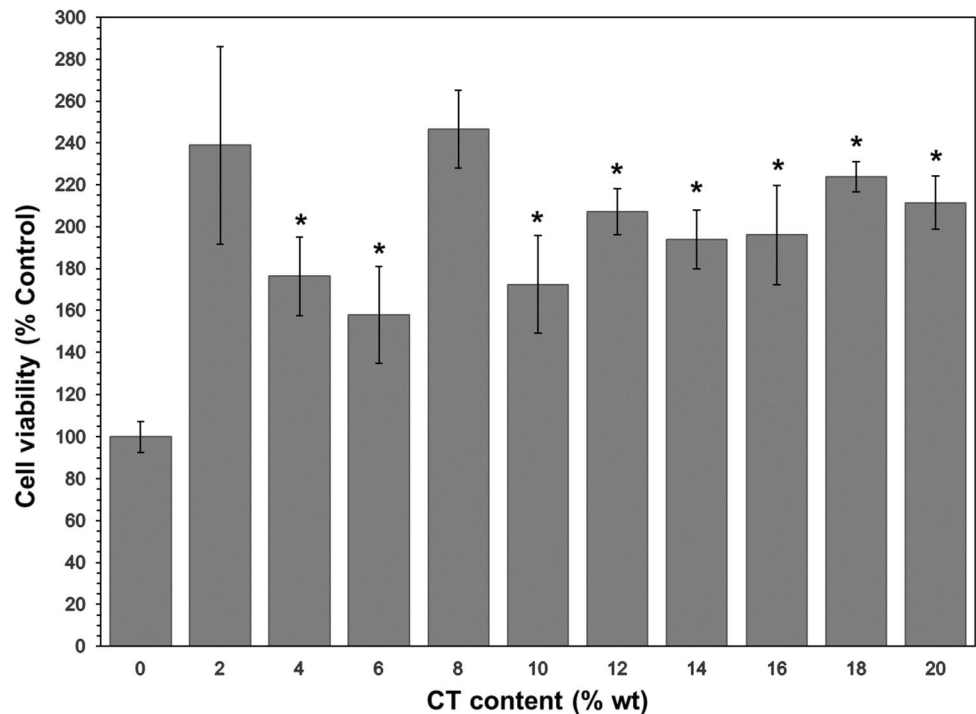
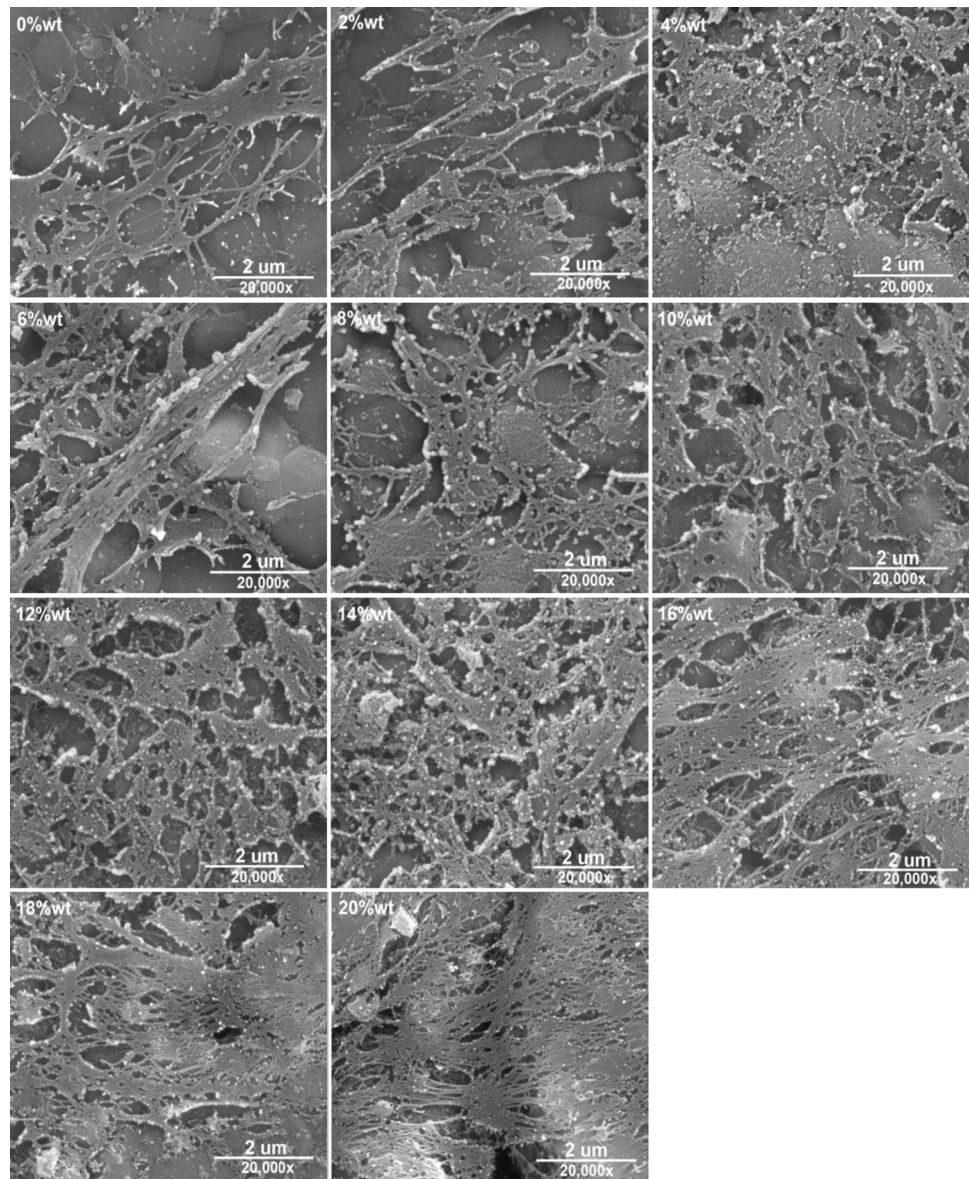


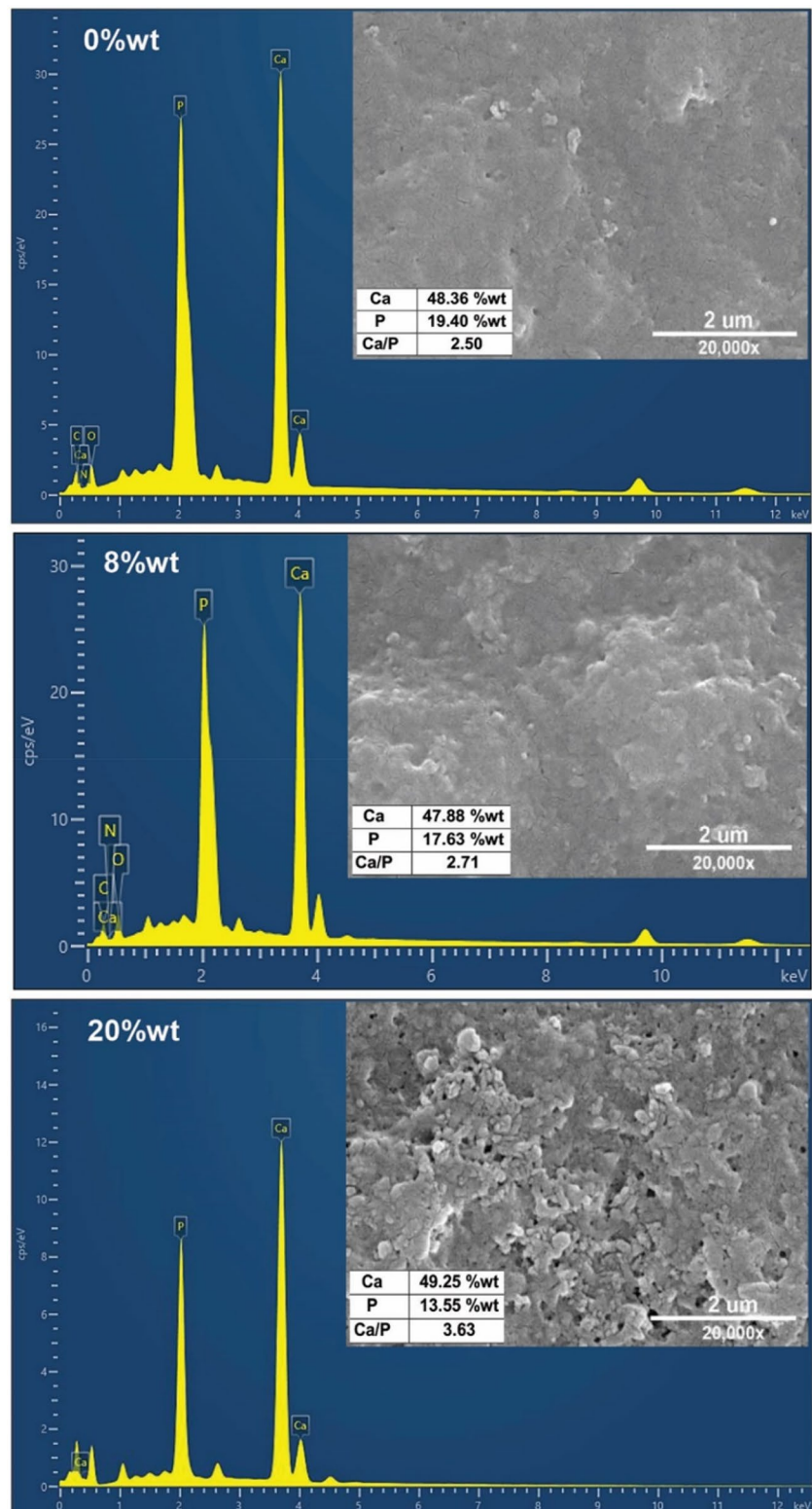
Fig. 18 SEM images of MC3T3-E1 osteoblast cells attached to hydroxyapatite and calcium titanate-hydroxyapatite composites at different calcium titanate contents after three days of culture



cells proliferated and spread with extended lamellipodia and filopodia. Cells could attach and form a cellular network on the composite surfaces, which indicated the biocompatibility of the composites and the promotion of tissue formation and growth. Although both HAp and the CT-HAp composites exhibited cell biocompatibility, the CT-HAp composite was more biocompatible than pure HAp since cellular proliferation and expansion were greater. The positive ion content of the composite surface and the surface morphology were factors that improved biocompatibility [6, 63]. The presence of highly conductive CT particles in the HAp matrix activated bioaffinity and the rougher and more irregular surface favored cell attachment.

The surfaces of HAp and CT-HAp samples soaked in CGM for seven days were observed by SEM. When compared to the original surfaces (Fig. 7), certain changes were observed. The surfaces of HAp and CT-HAp composites were covered with rough layers that grew perpendicularly to the surfaces and these layers were deposited with increasing thickness as CT content increased (Fig. 19). EDX analysis indicated that the Ca/P ratio of sample surfaces increased from 2.50 for HAp to 3.63 for 20%wtCT-HAp. A previous report suggested [65] that calcium and phosphate ions obtained from culture medium and/or from the vicinity of degraded ceramics were possibly precipitated as new calcium-phosphate onto the material surface.

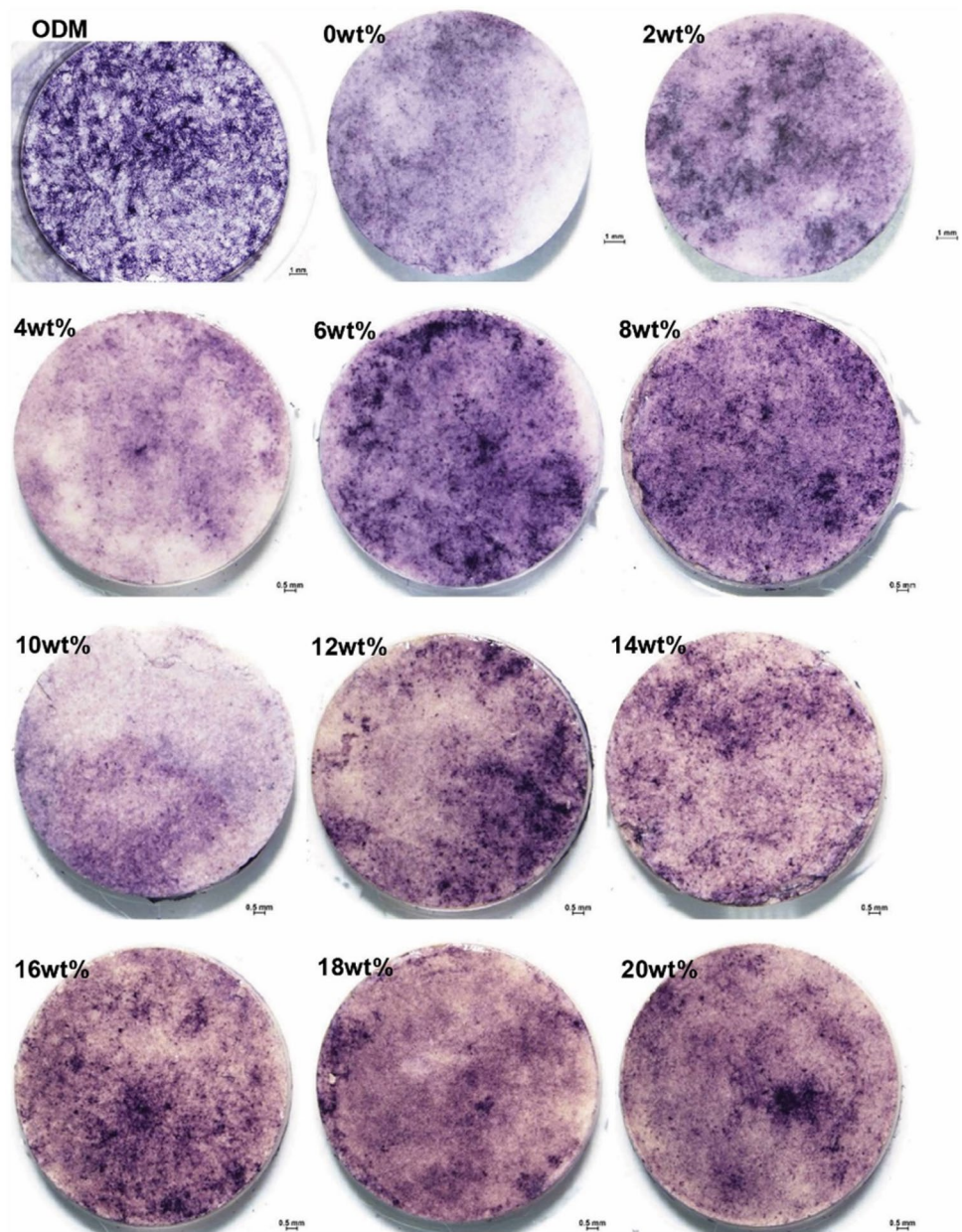
Fig. 19 SEM images-EDX profiles show the surface morphologies and chemical compositions of calcium titanate-hydroxyapatite composites with different calcium titanate contents. The images and analyses were obtained after osteogenic induction in osteogenic induction medium for 24 h followed by soaking in complete growth medium for seven days



ALP, a common osteogenic marker, was used to evaluate the growth of MC3T3-E1 osteoblast cells cultured in CGM for seven days after osteogenic induction (Fig. 20). Since

the original blue color of the stain, labeled with NBT/BCIP, was unchanged in ODM alone, no secretion of ALP occurred from the cells to ODM. Purple ALP staining

Fig. 20 Alkaline phosphatase activity in response to osteogenic induction in MC3T3-E1 osteoblast cells on hydroxyapatite and calcium titanate-hydroxyapatite composites at different calcium titanate contents was indicated by NBT/BCIP staining

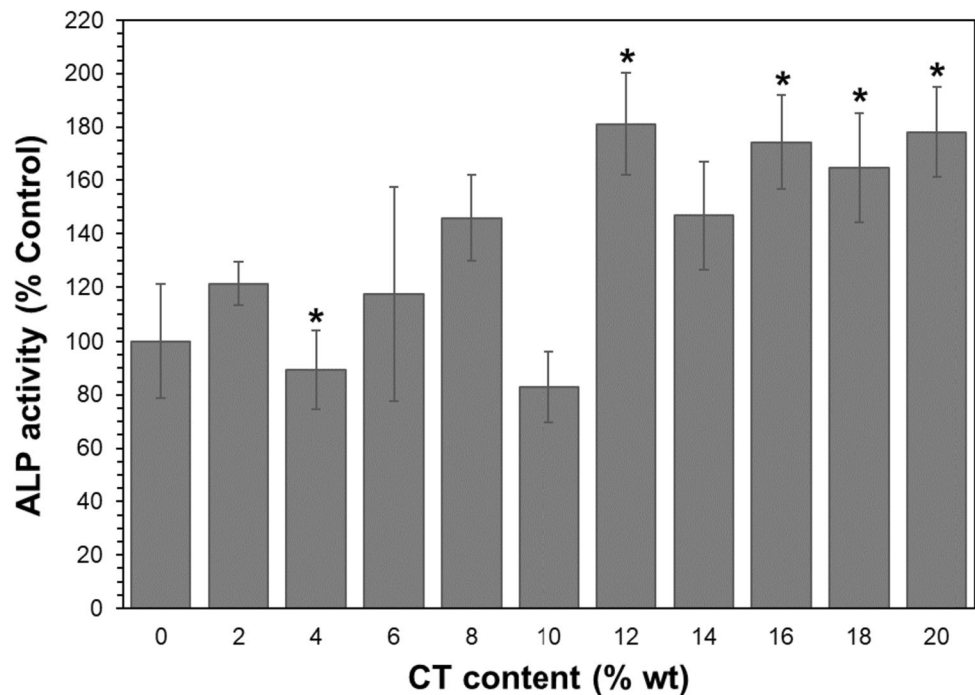


indicated the presence of MC3T3-E1 cells on all HAp and CT-HAp samples. However, the adherence of the cells varied at different contents of CT. The visual evidence was consistent with the response to osteogenic induction by ALP activity (Fig. 21). Zhang et al. [66] reported that CT enhanced the attachment and induced the spread and proliferation of MC3T3-E1 cells, and promoted ALP activity. Extracellular Ca^{2+} ions from CaTiO_3 increased intracellular Ca^{2+} ions, which induced the proliferation and differentiation of osteoblast cells [67, 68].

Conclusions

Calcium titanate-hydroxyapatite (CT-HAp) bioceramic composites were synthesized with various CT contents (0–20%wt) and sintered conventionally at 1250 °C for 2 h in air. The phase formation, morphology, physical, mechanical and biological properties of the fabricated composites were examined. Based on XRD analysis, the composites formed a stable phase of calcium titanate and hydroxyapatite without any phase transformation. Microstructural observations

Fig. 21 Alkaline phosphatase (ALP) activity on hydroxyapatite and calcium titanate-hydroxyapatite composites at different calcium titanate contents and its variations in response to osteogenic induction in MC3T3-E1 osteoblast cells was assessed under a stereomicroscope. *denotes a statistically significant difference with respect to control (0%wt of calcium titanate)



revealed that increasing the CT content of the composite promoted the agglomeration of CT. Differences in the densification and porosity of composites with different CT contents could be explained by the presence of a non-densifying phase (CT). In addition, the grain size of the composites was slightly affected by CT content. However, the results showed that a CT-HAp composite containing 8%wt of CT exhibited the best mechanical properties (flexural strength, hardness and fracture toughness). The very low solubility of all composites after 28 days incubation indicated that the proposed composite degraded very slowly. In-vitro biological studies showed that osteoblast cells were viable, adhered, spread, proliferated and expressed alkaline phosphatase on the CT-HAp composites. Moreover, the cells covered a greater surface area of the composite with increments of CT. Thus, the mechanical properties, biocompatibility and cellular osteoinduction of the proposed CT-HAp composite are suitable properties for application in bone tissue engineering.

Acknowledgements This work was financially supported by a Basic Research Grant from Prince of Songkla University under contract no. SCI6302056S and the Faculty of Science Research Fund, Prince of Songkla University, under contract no.1-2564-02-005. Sincere thanks and appreciation are extended to Mr. Thomas Duncan Coyne for editing and proofreading this paper.

Declarations

Conflict of interest The authors declare no conflict of interest.

References

- Inthong, S., Kamnong, M., Intatha, U., Intawin, P., Pengpat, K., Tunkasiri, T., Eitssayeam, S.: Phase, mechanical and bioactivity properties of hydroxyapatite-calcium titanate composite. *Mater. Res. Express.* **6**(2), 1–6 (2018). <https://doi.org/10.1088/2053-1591/aaec2>
- Hou, X., Zhang, L., Zhou, Z., Luo, X., Wang, T., Zhao, X., Lu, B., Chen, F., Zheng, L.: Calcium phosphate-based biomaterials for bone repair. *Funct. Biomater.* **13**(187), 1–39 (2022). <https://doi.org/10.3390/fbm13040187>
- Dubey, A.K., Tripathi, G., Basu, B.: Characterization of hydroxyapatite-perovskite (CaTiO_3) composites: Phase evaluation and cellular response. *J. Biomed. Mater. Res. B. Appl. Biomater.* **95**(2), 321–329 (2010). <https://doi.org/10.1002/jbm.b.31716>
- Dubey, A.K., Mallik, P.K., Kundu, S., Basu, B.: Dielectric and electrical conductivity properties of multi-stage spark plasma sintered HA- CaTiO_3 composites and comparison with conventionally sintered materials. *J. Eur. Ceram.* **33**, 3445–3453 (2013). <https://doi.org/10.1016/j.jeurceramsoc.2013.07.012>
- Mallik, P.K., Basu, B.: Better early osteogenesis of electroconductive hydroxyapatite-calcium titanate composites in a rabbit animal model. *J. Biomed. Mater. Res. A* **102A**(3), 842–851 (2014). <https://doi.org/10.1002/jbm.a.34752>
- Balin, N.T., Mondal, D., Lee, B.T.: In vitro study of CaTiO_3 -hydroxyapatite composites for bone tissue engineering. *ASAIO J.* **60**(6), 722–729 (2014). <https://doi.org/10.1097/MAT.000000000000126>
- Ravikumar, K., Mallik, P.K., Basu, B.: Twinning induced enhancement of fracture toughness in ultrafine grained hydroxyapatite-calcium titanate composites. *J. Eur. Ceram.* **36**(3), 805–815 (2016). <https://doi.org/10.1016/j.jeurceramsoc.2015.10.044>
- Ozturk, S., Yetmez, M.: Studies on characterization of bovine hydroxyapatite/ CaTiO_3 biocomposites. *Adv. Mater. Sci. Eng.* **2016**, 1–7 (2016). <https://doi.org/10.1155/2016/6987218>

9. Inthong, S., Sweatman, D.R., Eitssayeam, S., Tunkasiri, T.: Influence of sintering temperature on physical and mechanical properties of hydroxyapatite-calcium titanate composite. *Key Eng. Mater.* **805**, 65–70 (2019). <https://doi.org/10.4028/www.scientific.net/KEM.805.65>
10. Choy, M.T., Tang, C.Y., Chen, L., Law, W.C., Tsui, C.P., Lu, W.W.: Microwave assisted in situ synthesis of porous titanium/calcium phosphate composites and their in vitro apatite-forming capability. *Compos. B Eng.* **83**, 50–57 (2015). <https://doi.org/10.1016/j.compositesb.2015.08.046>
11. Trzaskowska, M., Vivcharenko, V., Przekora, A.: The impact of hydroxyapatite sintering temperature on its microstructural, mechanical, and biological properties. *Int. J. Mol. Sci.* **24**(5083), 1–21 (2023). <https://doi.org/10.3390/ijms24065083>
12. Pires, L.A., de Meira, C.R., Tokuhara, C.K., de Oliveira, F.A., Dainezi, V.B., Zardin Graeff, M.S., Fortulan, C.A., de Oliveira, R.C., Puppini-Rontani, R.M., Borges, A.F.S.: Wettability and pre-osteoblastic behavior evaluations of a dense bovine hydroxyapatite ceramics. *J. Oral Sci.* **62**(3), 259–264 (2020). <https://doi.org/10.2334/josnusd.19-0007>
13. Wu, S., Tu, B., Lin, J., Wang, Z., Wang, X., Shen, M., Hu, R.: Evaluation of the biocompatibility of a hydroxyapatite-CaTiO₃ coating in vivo. *Biocybern Biomed Eng.* **35**(4), 296–303 (2015). <https://doi.org/10.1016/j.bbe.2015.05.001>
14. Rodríguez, A.P., Sánchez, M.A., Felice, B., Zamora, M.L., Tsujigiwa, H., Takabatake, K., Kawai, H., Nakano, K., Nagatsuka, H.: In vitro efficacy of CaCO₃ content in CaTiO₃-CaCO₃ composites for bone growth. *J. Hard Tissue Biol.* **27**(3), 250–256 (2018). <https://doi.org/10.2485/jhtb.27.250>
15. Morris, J.P., Backeljau, T., Chapelle, G.: Shells from aquaculture: a valuable biomaterial, not a nuisance waste product. *Rev. Aquac.* **11**(1), 42–57 (2019). <https://doi.org/10.1111/raq.12225>
16. Islam, K.N., Bakar, M.Z.B.A., Noordin, M.M., Hussein, M.Z.B., Abd Rahman, N.S.B., Ali, M.E.: Characterisation of calcium carbonate and its polymorphs from cockle shells (Anadara granosa). *Powder Technol.* **213**(1–3), 188–191 (2011). <https://doi.org/10.1016/j.powtec.2011.07.031>
17. Mohamed, M., Yusup, S., Maitra, S.: Decomposition study of calcium carbonate in cockle shell. *J. Eng. Sci. Technol.* **7**(1), 1–10 (2012). <https://doi.org/10.1016/j.jclepro.2012.07.050>
18. Hamester, M.R.R., Balzer, P.S., Becker, D.: Characterization of calcium carbonate obtained from oyster and mussel shells and incorporation in polypropylene. *Mater. Res.* **15**(2), 204–208 (2012). <https://doi.org/10.1590/S1516-14392012005000014>
19. Seesanong, S., Boonchom, B., Chaiseeda, K., Boonmee, W., Lao-havisuti, N.: Conversion of bivalve shells to monocalcium and tricalcium phosphates: An approach to recycle seafood wastes. *Materials.* **14**(4395), 1–15 (2021). <https://doi.org/10.3390/ma14164395>
20. Azis, Y., Jamarun, N., Arief, S., Nur, H.: Facile synthesis of hydroxyapatite particles from cockle shells (Anadara granosa) by hydrothermal method. *Orient. J. Chem.* **31**(2), 1–7 (2015). <https://doi.org/10.13005/ojc/310261>
21. Azis, Y., Jamarun, N., Zultinari, Arief, S., Nur, H.: Synthesis of hydroxyapatite by hydrothermal method from cockle shell (Anadara granosa). *J. Chem. Pharm. Res.* **7**(5), 798–804 (2015)
22. Khiri, M.Z.A., Matori, K.A., Zainuddin, N., Abdullah, C.A.C., Alassan, Z.N., Baharuddin, N.F., Zaid, M.H.M.: The usability of ark clam shell (Anadara granosa) as calcium precursor to produce hydroxyapatite nanoparticle via wet chemical precipitate method in various sintering temperature. *Springerplus.* **5**(1206), 1–15 (2016). <https://doi.org/10.1186/s40064-016-2824-y>
23. Ferdynanto, R.A., Dharmayanti, P.E.S., Dewi, P.T.K., Prananingrum, W.: The effect of various concentrations of HA-TCP derived from cockle shell synthesis on scaffold porosity. *Dent. J.* **51**(3), 114–118 (2018). <https://doi.org/10.20473/j.djmg.v51.i3.p114-118>
24. Saharudin, S.H., Shariffuddin, J.H., Nordin, N.I.A.A., Ismail, A.: Effect of aging time in the synthesis of biogenic hydroxyapatite derived from cockle shell. *Mater. Today: Proc.* **19**(4), 1208–1215 (2019). <https://doi.org/10.1016/j.matpr.2019.11.124>
25. Fatimah, I., Fahrani, D., Harmawantika, T., Sahroni, I., Kamari, A., Rahmatillah, C.S., Nurillahi, R.: Functionalization of hydroxyapatite derived from cockle (Anadara granosa) shells into hydroxyapatite-nano TiO₂ for photocatalytic degradation of methyl violet. *Sustain. Environ. Res.* **29**(40), 1–14 (2019)
26. Mohd Puad, N.A.S., Te Chuan, L., Salman, N.S., Selimin, M.A., Abdul Latif, A.F., Muhamad, M.S., Abdullah, H.Z., Idris, M.I., Mustapha, S.N.H.: Synthesis of bioactive calcium phosphate from cockle shell for biomedical applications. *Biointerface Res. Appl. Chem.* **10**(4), 5787–5791 (2020). <https://doi.org/10.33263/BRIAC104.787791>
27. Sinurat, E., Dewi, F.R., Fransiska, D., Nurbayasari, R.: Synthesis and characterization of hydroxyapatite of cockle shells (Anadara granosa) originated from Indonesia through precipitation method. *IOP Conf. Ser.: Earth Environ.* **1118**(012035), 1–12 (2022). <https://doi.org/10.1088/1755-1315/1118/1/012035>
28. Mtavangu, S.G., Mahene, W., Machunda, R.L., Van der Bruggen, B., Njau, K.N.: Cockle (Anadara granosa) shells-based hydroxyapatite and its potential for defluoridation of drinking water. *Results Eng.* **13**(100379), 1–16 (2022). <https://doi.org/10.1016/j.rineng.2022.100379>
29. Fatimah, I., Nur Ilahi, R., Pratami, R.: Low cost CaTiO₃ perovskite synthesized from scallop (Anadara granosa) shell as antibacterial ceramic material. *IOP Conf. Ser.: Mater. Sci. Eng.* **299**(012034), 1–6 (2022). <https://doi.org/10.1088/1757-899X/299/1/012034>
30. Ozawa, M., Hattori, M., Satake, K.: *Waste management and application of fish bone hydroxyapatite for waste water treatment*. Proc. of International Symposium on EcoTopia Science, (2007), p. 957–958
31. Cherdchom, S., Rattanaphan, T., Chanadee, T.: Calcium titanate from food waste: combustion synthesis, sintering, characterization, and properties. *Adv. Mater. Sci. Eng.* **2019**, 1–10 (2019). <https://doi.org/10.1155/2019/9639016>
32. Maitreekeaw, K., Chanadee, T.: Calcium titanate ceramics obtained by combustion synthesis and two-step sintering. *Sci. Sinter.* **52**, 491–502 (2020). <https://doi.org/10.2298/SOS2004491M>
33. Sri-o-sot, S., Vepulanont, K., Kamkit, C., Srichumpong, T., Chanadee, T.: Fabrication, characterization, and properties of hydroxyapatite ceramics derived from cockle shell. *J. Aust. Ceram. Soc.* **58**, 1081–1093 (2022). <https://doi.org/10.1007/s41779-022-00757-8>
34. Čorić, D., Čurković, L., Majić Renjo, M.: Statistical analysis of vickers indentation fracture toughness of Y-TZP ceramics. *Trans. Famena.* **41**(2), 1–16 (2017). <https://doi.org/10.21278/TOF.41201>
35. Callister, W.D., Rethwisch, D.G.: *materials science and engineering: an introduction*. Wiley, USA (2018)
36. Kokubo, T., Takadama, H.: How useful is SBF in predicting in vivo bone bioactivity? *Biomaterials* **27**, 2907–2915 (2006). <https://doi.org/10.1016/j.biomaterials.2006.01.017>
37. Liu, X., Sun, Y., Chen, B., Li, Y., Zhu, P., Wang, P., Yan, S., Li, Y., Yang, F., Gu, N.: Novel magnetic silk fibroin scaffolds with delayed degradation for potential long-distance vascular repair. *Bioact. Mater.* **7**, 126–143 (2022). <https://doi.org/10.1016/j.bioactmat.2021.04.036>
38. Louis, K.S., Siegel, A.C.: Cell viability analysis using trypan blue: manual and automated methods. In: Stoddart, M. (ed.) *Mammalian cell viability*. Methods in molecular biology, vol. 740, pp. 7–12. Humana Press, New York (2011). https://doi.org/10.1007/978-1-61779-108-6_2
39. Dogan, S.C., Polat, Z.A., Deren, S., Yayci, S.F.: Cetin. Effects of neuromuscular blocking drugs on viability of human umbilical vein endothelial cells (HUVECs). *Int. J. Med. Res.* **48**(6), 1–7 (2020). <https://doi.org/10.1177/0300060520910888>
40. Chatree, K., Sriboonaied, P., Phetkong, C., Wattananit, W., Chanchao, C., Charoenpanich, A.: Distinctions in bone matrix

- nanostructure, composition, and formation between osteoblast-like cells, MG-63, and human mesenchymal stem cells, UE7T-13. *Heliyon*. **9**, 1–16 (2023). <https://doi.org/10.1016/j.heliyon.2023.e15556>
41. Suchanek, W., Yoshimura, M.: Processing and properties of hydroxyapatite-based biomaterials for use as hard tissue replacement implants. *J. Mater. Res.* **13**(1), 94–117 (1998). <https://doi.org/10.1557/JMR.1998.0015>
 42. Xie, J., Ye, Q., Zhou, J., Liao, Y., Qian, G.: The photocatalytic activity of CaTiO₃ derived from the microwave-melting heating process of blast furnace slag. *Nanomaterials*. **13**(1412), 1–16 (2023). <https://doi.org/10.3390/nano13081412>
 43. Bulina, N.V., Makarova, S.V., Baev, S.G., Matvienko, A.A., Gerasimov, K.B., Logutenko, O.A., Bystrov, V.S.: A Study of thermal stability of hydroxyapatite. *Minerals*. **11**(1310), 1–15 (2021). <https://doi.org/10.3390/min11121310>
 44. Gralik, G., Thomsen, A.E., Moraes, C.A., Raupp-Pereira, F., Hotza, D.: Processing and characterization of CaTiO₃ perovskite ceramics. *Process. Appl. Ceram.* **8**(2), 53–57 (2014). <https://doi.org/10.2298/PAC1402053G>
 45. Ramírez, M.A., Parra, R., Reboredo, M.M., Varela, J.A., Castro, M.S., Ramajo, L.: Elastic modulus and hardness of CaTiO₃, CaCu₃Ti₄O₁₂ and CaTiO₃/CaCu₃Ti₄O₁₂ mixture. *Mater. Lett.* **64**, 1226–1228 (2010). <https://doi.org/10.1016/j.matlet.2010.02.058>
 46. Aswad, M.A.: Measurement of the fracture toughness and mechanical properties of hydroxyapatite using vickers indentation technique. *Nanosistemi, Nanomateriali, Nanotehnologii*. **19**(3), 571–584 (2021)
 47. Hervas, I., Montagne, A., Van Gorp, A., Bentoumi, M., Thuault, A.A.: lost. Fracture toughness of glasses and hydroxyapatite: A comparative study of 7 methods by using vickers indenter. *Ceram. Inter.* **42**(11), 12740–12750 (2016). <https://doi.org/10.1016/j.ceramint.2016.05.030>
 48. Quinn, J.B., Quinn, G.D.: On the hardness and brittleness of ceramics. *Key Eng. Mater.* **132–136**, 460–463 (1997). <https://doi.org/10.1002/9780470314821.ch7>
 49. Miranda-Hernandez, J.G., Vargas-Hernandez, J., Casarrubias-Vargas, H., Gonzalez-Moran, C.O., Refugio-García, E., de Jesús, J., Flores Cuautle, A.: Synthesis and effect of CaTiO₃ formation in CaO·Al₂O₃ by solid-state reaction from CaCO₃·Al₂O₃ and Ti. *Mater. Chem. Phys.* **232**, 57–64 (2019). <https://doi.org/10.1016/j.matchemphys.2019.04.050>
 50. Cziko, M., Bogy, E.S., Barabás, R., Bizo, L., Stefan, R.: In vitro biological activity comparison of some hydroxyapatite-based composite materials using simulated body fluid. *Cent. Eur. J. Chem.* **11**(10), 1583–1598 (2013). <https://doi.org/10.2478/s11532-013-0293-5>
 51. So, K., Fujibayashi, S., Neo, M., Anan, Y., Ogawa, T., Kokubo, T., Nakamura, T.: Accelerated degradation and improved bone-bonding ability of hydroxyapatite ceramics by the addition of glass. *Biomaterials* **27**, 4738–4744 (2006). <https://doi.org/10.1016/j.biomaterials.2006.05.020>
 52. Shuai, C., Yang, W., Feng, P., Peng, S., Pan, H.: Accelerated degradation of HAP/PLLA bone scaffold by PGA blending facilitates bioactivity and osteoconductivity. *Bioact. Mater.* **6**, 490–502 (2021). <https://doi.org/10.1016/j.bioactmat.2020.09.001>
 53. Vlădescu, A., Pârâu, A., Pană, I., Cotrut, C.M., Constantin, L.R., Vlădescu, A., Pârâu, A., Pană, I., Cotrut, C.M., Constantin, L.R.: In vitro activity assays of sputtered HAp coatings with SiC addition in various simulated biological fluids. *Coatings* **9**(383), 1–17 (2019). <https://doi.org/10.3390/coatings9060389>
 54. Jeong, J., Kim, J.H., Shim, J.H., Hwang, N.S., Heo, C.Y.: Bioactive calcium phosphate materials and applications in bone regeneration. *Biomater. Res.* **23**(4), 1–11 (2019). <https://doi.org/10.1186/s40824-018-0149-3>
 55. Hsu, P.Y., Kuo, H.C., Tuan, W.H., Shih, S.J., Naito, M., Lai, P.L.: Manipulation of the degradation behavior of calcium sulfate by the addition of bioglass. *Prog. Biomater.* **8**, 115–125 (2019). <https://doi.org/10.1007/s40204-019-0116-7>
 56. Sanchez, Mate, de Val, J.E., Calvo-Guirado, J.L., Gomez-Moreno, G., Perez-Albacete Martinez, C., Mazon, P., De Aza, P.N.: Influence of hydroxyapatite granule size, porosity, and crystallinity on tissue reaction in vivo. Part A: synthesis, characterization of the materials, and SEM analysis. *Clin. Oral. Impl. Res.* **27**(11), 1331–1338 (2016). <https://doi.org/10.1111/clr.12722>
 57. Pattanayak, D.K., Prasad, R.C., Rao, B.T., Rama Mohan, T.R.: Apatite wollastonite-titanium biocomposites: Synthesis and in vitro evaluation. *J. Am. Ceram. Soc.* **89**(7), 2172–2176 (2006). <https://doi.org/10.1111/j.1551-2916.2006.01068.x>
 58. Jamaludin, S.B., Shima Adzali, N.M., Nazree Derman, M.: Microstructure and in-vitro test bioactivity behavior of Co-CrMo (F-75)/hydroxyapatite in phosphate buffered saline solution. *Acta Metall. Slovaca*. **20**(1), 82–88 (2014). <https://doi.org/10.12776/ams.v20i1.192>
 59. Wan, Y.Z., Hong, L., Jia, S.R., Huang, Y., Zhu, Y., Wang, Y.L., Jiang, H.J.: Synthesis and characterization of hydroxyapatite-bacterial cellulose nanocomposites. *Compos. Sci. Technol.* **66**, 1825–1832 (2006). <https://doi.org/10.1016/j.compscitech.2005.11.027>
 60. Yang, Z., Xia, L., Li, W., Han, J.: Effect of Ca/P ratio on bioactivity of PEO coatings. *Adv. Biomed. Eng.* **2**, 13–19 (2015). <https://doi.org/10.15379/2409-3394.2015.02.01.2>
 61. Hassan Ibrahim, A.M., Takacova, M., Jelenska, L., Csaderova, L., Balog, M., Kopacek, J., Svastova, E., Krizik, P.: The effect of surface modification of TiMg composite on the in-vitro degradation response, cell survival, adhesion, and proliferation. *Mater. Sci. Eng. C* **127**, 1–11 (2021). <https://doi.org/10.1016/j.msec.2021.112259>
 62. Dziadek, M., Zagrajczuk, B., Menaszek, E., Cholewa-Kowalska, K.: A new insight into in vitro behaviour of poly(ϵ -caprolactone)/bioactive glass composites, in biologically related fluids. *J. Mater. Sci.* **53**, 3939–3958 (2018). <https://doi.org/10.1007/s10853-017-1839-2>
 63. Thrivikraman, G., Mallik, P.K., Basu, B.: Substrate conductivity dependent modulation of cell proliferation and differentiation in vitro. *Biomaterials* **34**, 7073–7085 (2013). <https://doi.org/10.1016/j.biomaterials.2013.05.076>
 64. Deligianni, D.D., Katsala, N.D., Koutsoukos, P.G., Missirlis, Y.F.: Effect of surface roughness of hydroxyapatite on human bone marrow cell adhesion, proliferation, differentiation and detachment strength. *Biomaterials* **22**, 87–96 (2001). [https://doi.org/10.1016/s0142-9612\(00\)00174-5](https://doi.org/10.1016/s0142-9612(00)00174-5)
 65. Zhang, J., Luo, X., Barbieri, D., Barradas, A.M.C., de Bruijn, J.D., van Blitterswijk, C.A., Yuan, H.: The size of surface microstructures as an osteogenic factor in calcium phosphate ceramics. *Acta Biomater.* **10**(7), 3254–3263 (2014). <https://doi.org/10.1016/j.actbio.2014.03.021>
 66. Zhang, Y., Wang, K., Dong, K., Cui, N., Lu, T., Han, Y.: Enhanced osteogenic activity of poly ether ether ketone using calcium plasma immersion ion implantation. *Colloids Surf. B* **187**, 1–10 (2020). <https://doi.org/10.1016/j.colsurfb.2016.02.056>
 67. Zayzafoon, M.: Calcium/calmodulin signaling controls osteoblast growth and differentiation. *J. Cell. Biochem.* **97**, 56–70 (2006). <https://doi.org/10.1002/jcb.20675>
 68. Hu, J., Zhou, Y., Huang, L., Liu, J., Lu, H.: Effect of nano-hydroxyapatite coating on the, osteoinductivity of porous biphasic calcium phosphate ceramics. *BMC Musculoskelet. Disord.* **15**(114), 1–13 (2014). <https://doi.org/10.1186/1471-2474-15-114>

Publisher's Note Springer Nature remains neutral with regard to jurisdictional claims in published maps and institutional affiliations.

Springer Nature or its licensor (e.g. a society or other partner) holds exclusive rights to this article under a publishing agreement with the author(s) or other rightsholder(s); author self-archiving of the accepted manuscript version of this article is solely governed by the terms of such publishing agreement and applicable law.